Airborne and spaceborne remote sensing for assessment of forest structural attributes across tropical mosaic landscapes

HARI ADHIKARI

ACADEMIC DISSERTATION
To be presented, with the permission of the Faculty of Science of
the University of Helsinki, for public examination in Auditorium CK 112 of
the Exactum building of the University of Helsinki, on 4th October 2019, at 12 noon.

DEPARTMENT OF GEOSCIENCES AND GEOGRAPHY A70 / HELSINKI 2019

Author's address: Hari Adhikari
Department of Geosciences and Geography
P.O. Box 64, FIN-00014 University of Helsinki, Finland
hari.adhikari@helsinki.fi

Supervisors: Professor Petri Pellikka
Department of Geosciences and Geography
University of Helsinki, Finland

Dr. Janne Heiskanen
Institute for Atmospheric and Earth System Research /
Department of Geosciences and Geography
University of Helsinki, Finland

Pre-examiners: Associate Professor Timo Kumpula
Department of Geographical and Historical Studies
University of Eastern Finland, Finland

Dr. Achim Röder
Institute of Spatial and Environmental Sciences
Trier University, Germany

Opponent: Professor Kevin Tansey
School of Geography, Geology and the Environment
University of Leicester, Great Britain

ISSN-L 1798-7911
ISSN 1798-7911 (print)
ISBN 978-951-51-3993-1 (paperback)
ISBN 978-951-51-3994-8 (PDF)
http://ethesis.helsinki.fi

Unigrafia
Helsinki 2019

In memory of my brother (Niranjan Adhikari [Santosh])

Adhikari, H., (2019). Airborne and spaceborne remote sensing for assessment of forest structural attributes across tropical mosaic landscapes. Department of Geosciences and Geography, University of Helsinki, A70. Unigrafia, Helsinki.

Abstract

High-resolution, accurate, and updated forest structure maps are urgently required for the implementation of REDD+, payment of ecosystem services, and other climate change mitigation strategies in tropical countries. The collection of forest inventory data is usually labor intensive and costly, and remote sites can be difficult to access. Remote sensing data, for example airborne laser scanning (ALS), hyperspectral imagery, and Landsat data, complement field-based forest inventories and provide high-resolution, accurate, and spatially explicit data for mapping forest structural attributes. However, issues such as the effect of topography, pulse density, and the single and combined use of various remote sensing data on forest structural attributes prediction warrant further research.

The main objective of this thesis was to assess airborne and spaceborne remote sensing techniques for modeling forest structural attributes across a montane forest landscape in the Taita Hills, Kenya. The sub-objectives focused on a) the effect of the topographic normalization of Landsat images on fractional cover (Fcover) prediction, aboveground biomass (AGB), and forest structural heterogeneity modeling using ALS and other remote sensing data and b) the analysis of the maps of forest structural attributes.

In Study I, the effect of topographic normalization on ALS-based Fcover modeling was evaluated using common vegetation indices and spectral-temporal metrics based on a Landsat time series (LTS). The results demonstrate that the fit of the Fcover models did not improve after topographic normalization in the case of ratio-based vegetation indices (Normalized Difference Vegetation Index, NDVI; reduced simple ratio, RSR) or tasseled cap (TC) greenness; however, the fit improved in the case of brightness and wetness, particularly in the period of the lowest sun elevation. However, if TC indices are preferred, then topographic normalization using a Shuttle Radar Topography Mission (SRTM) digital elevation model (DEM) is recommended.

In Study II, field-based AGB estimates are modeled by ALS data and a multiple linear regression. The plot-level AGB was modeled with a coefficient of determination (R^2) of 0.88 and a root mean square error (RMSE) of 52.9 Mg ha^{-1}. Furthermore, the determinants for AGB spatial distribution are examined using geospatial data and statistical modeling. The AGB patterns are controlled mainly by mean annual precipitation (MAP), the distribution of croplands, and slope, which collectively explained 69.8% of the AGB variation.

Study III investigated whether the fusion of ALS with LTS and hyperspectral data, or stratification of the plots to the forest and non-forest classes, improves AGB modeling. According to the results, the prediction model based on ALS data only provides accurate models even without stratification. However,

using ALS and HS data together, and employing an additional forest classification for stratification, improves the model accuracy considerably in the studied landscape.

Finally, in Study IV, the potential of single and combined ALS and LTS data in modeling forest structural heterogeneity (the Gini coefficient of tree size) was assessed, and the difference between three forest remnants and forest types is evaluated based on predicted maps. If the LTS metrics were included in the models, then ALS data with lower pulse density yield similar accuracy to more expensive, high pulse-density data. Furthermore, the GC map presents forest structural heterogeneity patterns at the landscape scale and demonstrates the importance of remote sensing-based maps over information based on field plots only.

This thesis provides new insights into the modeling and analyzing of forest structural attributes based on airborne and spaceborne remote sensing data. The results demonstrate that ALS data alone provide robust models for AGB and GC mapping in the tropical agriculture-forest mosaic landscape and small forest remnants. However, important synergies exist between remote sensing data sets. Therefore, fusion of ALS, HS, and LTS data for the prediction of plot-level forest structural attributes appears to be a promising approach for landscape-level applications.

Photo: © Prof. Petri Pellikka

Acknowledgements

This thesis was accomplished at the Department of Geosciences and Geography, University of Helsinki in a beautiful city of Helsinki, a city of bright future, kind hearted human, full of natural beauty and fresh air.

I would like to deeply express my gratitude to my supervisor Professor Petri Pellikka for accepting me as a PhD student in University of Helsinki. He patiently transferred me his knowledge of remote sensing, and organized the funding which enabled me to concentrate on this thesis. He has been on my side for every problem I have solved, for every success I have achieved and every sorrow I have gone through. He is not only my Professor but also a guardian during my stay in Finland.

I would like to express my gratitude to my co-supervisor Dr. Janne Heiskanen. You have been very supportive to me and I would not have completed this PhD without your help. I could reach you on every minutes of the day and every day of the year. Your in-depth knowledge on every aspect of my research helped me a lot.

I am grateful to my co-authors Dr. Eduardo Maeda, Dr. Mika Siljander, Vuokko Heikinheimo, and Dr. Rami Piiroinen (Department of Geosciences and Geography, University of Helsinki), Dr. Ruben Valbuena (School of Natural Sciences, Bangor University) and Prof. Petteri Packalen (School of Forest Sciences, University of Eastern Finland). Without their kind cooperation, this thesis could not exist. You have been there for me whenever I knock your door and you provided me plenty of information on my queries.

Special thanks go to Prof. Mikael Fortelius for involving me in an interesting project (ECHOES) and supporting and encouraging me to achieve the destination.

I would like to thank the two pre-examiners of this thesis, Associate Professor Timo Kumpula and Dr. Achim Röder for allocating your precious time to review my thesis and providing constructive comments. I also would like to thank all the colleagues Jinxiu, Rami, Zhipeng, Antti, Yang, Sheila, Peifeng, Pekka, Edward, Temesgen, Daniela, Yanlong, Vincent, Zou, Viljami, Jesse, Andrew, Binyam, Elisa, Rocio, Vuokko, Tino, Arttu, Mikko, Janina and Indre for your continuous support. Jinxiu (Jenny) you have been always like my sister, best friend, and a nice officemate. I also would like to thank my friends and families in Finland and abroad for their support and care.

The Taita Research Station of the University of Helsinki is gratefully acknowledged for logistical support. I would like to thank all the staff at the station and field guides including James Mwang'ombe, Mwadime Mjomba, Granton Righa, Darius Kimuzi, Francis Namiseko, Rebecca Mwanyolo, Damaris, Julius, Ken Gicheru and Elphinstone Kalaghe. Special thanks to Darius and Mwadime, without your help I would not have been able to collect precious ground truth field inventory data.

This thesis would not have been completed without the funding and support from 1) Center for International Mobility (CIMO of Finland), 2) Climate Change Impact Detection and Monitoring Adaptation Measures - Development of Remote-Sensing Tools (ALPS), 3) Geoinformatics in Monitoring and Modelling Environment Change (GIMMEC), 4) Doctoral school grant and travel grant from ATM-DP doctoral school, and 5) The Ecological Context of Human Origins and its Evolutionary Significance: Six Million Years of Changing Herbivore Resource Use in the Turkana Basin (ECHOES) and 6) SMARTLAND – Environmental sensing of ecosystem services for developing climate smart landscape framework to improve food security in East Africa. Research permit from the National Council for Science and Technology of Kenya is gratefully acknowledged.

Finally, I am deeply indepted to my family, son Eric, unborned child (Evhan), wife Namrata and my family members, Dharmaraj, Sharada, Sharad, Rekha, Shrey, Shreya, Kalpana, deceased Niranjan (12.09.2016), Rikhiram, Laxmidevi, Neelam, Netu, Nisha, Nikita, Yubraj, Sujit, Ramesh, Rahul, Rohit for their unconditional love and endless support. Special thanks to my wife who always supported me on every steps of my PhD. It would not have been possible to complete my PhD without you.

Contents

Abstract 5
Acknowledgements 7
Contents 9
List of original publications 10
Abbreviations 11
List of figures and tables 12

1 **Introduction** 13
2 **Background** 17
2.1 Medium-resolution satellite image time series: importance of topographic normalization 17
2.2 Modeling forest structural attributes using multi-source remote sensing data 18
2.3 Analyzing maps of forest attributes 20
3 **Material and methods** 22
3.1 Study area 22
3.2 Field data 23
3.3 Remote sensing datasets 24
3.3.1 Airborne laser scanning (ALS) data 24
3.3.2 Hyperspectral sensor (HS) data 26
3.3.3 Multispectral spaceborne (MS) data 26
3.3.4 Digital elevation models (DEMs) and digital surface model (DSM) 26
3.3.5 Auxiliary data 28
3.4 Preprocessing and image compositing 28
3.5 Modeling 28
3.6 Statistical analysis 30
4 **Results and discussion** 31
4.1 Effect of topographic normalization 31
4.2 Prediction of forest structure attributes at landscape scale: benefits of data fusion 33
4.3 Explanation of above ground biomass (AGB) distribution and forest tree size inequality based on maps 39
4.4 Limitations and topics for further studies 41
5 **Conclusions** 42
References 44

List of original publications

This thesis is based on the following publications:

I **Adhikari, H.**, Heiskanen, J., Maeda, E. E., & Pellikka, P. K. E. (2016). The effect of topographic normalization on fractional tree cover mapping in tropical mountains: An assessment based on seasonal Landsat time series. International Journal of Applied Earth Observation and Geoinformation, 52, 20-31. http://dx.doi.org/10.1016/j.jag.2016.05.008

II **Adhikari, H.**, Heiskanen, J., Siljander, M., Maeda, E., Heikinheimo, V., & Pellikka, P. K. E. (2017). Determinants of aboveground biomass across an Afromontane landscape mosaic in Kenya. Remote Sensing, 9(8), 827. http://dx.doi.org/10.3390/rs9080827

III Heiskanen, J., **Adhikari, H.**, Piiroinen, R., Packalen, P., Pellikka, P. K. E. (2019). Do airborne laser scanning biomass prediction models benefit from Landsat time series, hyperspectral data or forest classification in tropical mosaic landscapes? International Journal of Applied Earth Observation and Geoinformation, 81, 176-185. https://doi.org/10.1016/j.jag.2019.05.017.

IV **Adhikari, H.**, Valbuena, R., Pellikka, P. K. E., Heiskanen, J. (2020). Mapping forest structural heterogeneity of montane forest remnants from airborne laser scanning and Landsat spectral-temporal metrics. Ecological Indicators, 108, 105739. https://doi.org/10.1016/j.ecolind.2019.105739.

Authors's contribution

	I	II	III	IV
Conceive and design study	HA, JH, EM	HA, JH, MS	JH, HA	HA, JH, RV
Field data collection		JH, HA, PPE, VH	JH, PPE	HA, JH, PPE
Remote sensing data collection and processing	HA, PPE, JH	PPE, JH, HA	PPE, JH, HA, RP	PPE, JH, HA
Data analysis	HA, JH, EM	HA, JH, MS	JH, HA, PP	HA, JH, RV
Manuscript preparation	HA, JH, EM	HA, JH, EM, MS, PPE, VH	JH, HA, PP, RP	HA, JH, RV, PPE

HA = Hari Adhikari; JH = Janne Heiskanen; PPE = Petri K. E. Pellikka;

EM = Eduardo Maeda; RV = Ruben Valbuena; MS = Mika Siljander;

PP = Petteri Packalen; RP = Rami Piiroinen; VH = Vuokko Heikinheimo

Abbreviations

ABA	Area-based approach
AGB	Aboveground biomass
AGC	Aboveground carbon
AISA	Airborne Imaging Spectroscopy Application
ALS	Airborne laser scanning
ASTER	Advanced Spaceborne Thermal Emission and Reflection Radiometer
Brightness	Tasseled cap Brightness
BRT	Boosted regression tree
CHM	Canopy height model
DBH	Diameter at breast height
DEM	Digital elevation model
DSM	Digital surface model
EAM	Eastern Arc Mountain Range
ETM+	Landsat 7 Enhanced Thematic Mapper Plus
Fcover	Fractional tree cover
GC	Gini coefficient
GIS	Geographic information system
Greenness	Tasseled cap Greenness
HRVIR	High Resolution Visible Infrared
HS	Hyperspectral sensor (Imaging Spectroscopy)
LiDAR	Light Detection and Ranging
LOOCV	Leave one out cross-validation
LTS	Landsat time series
MAP	Mean annual precipitation (mm)
MAT	Mean annual temperature (°C)
MODIS	Moderate Resolution Imaging Spectroradiometer
NDVI	Normalized Difference Vegetation Index
NIR	Near-infrared
OLI	Landsat 8 Operational Land Imager
R^2	The coefficient of determination
REDD+	Reducing Emissions from Deforestation and Forest Degradation
RMSE	Root mean square error
RS	Remote sensing
RSR	Reduced Simple Ratio
SRTM	Shuttle Radar Topography Mission
SWIR	Shortwave infrared
TM	Thematic Mapper
TOPO	Regional DEM based on topographic maps
TPI	Topographic Position Index
TWI	Topographic Wetness Index
UTM	Universal Transverse Mercator
Wetness	Tasseled cap Wetness
WGS	World Geodetic System

List of figures and tables

Figure 1. The main contents of the thesis and four studies (I–IV).....16

Figure 2. (Left) False color composite of individual Landsat-7 Enhanced Thematic Mapper Plus (ETM+) image available during a one-year time period. The white areas represent clouds and cloud shadows masked from the image, and white lines represent scan line corrector off (SLC-off). (Right) Examples of spectral-temporal metrics (various percentile, trimmed mean, interpercentile, and interquartile ranges) based on tasseled cap transformation (brightness).....18

Figure 3. Location of the Taita Hills study area with Sentinel-2A multi spectral instrument satellite image from 8 October, 2016 in the background. The area covered by the blue box represents airborne laser scanning (ALS1) and hyperspectral image coverage (10,000 ha), and the black box represents ALS2 coverage (~55,000 ha). See additional details about ALS (1 and 2) in Table 2....22

Figure 4. Overview of the methodology.....25

Figure 5. (a) Relationship between the Gini coefficient (GC) and the Lorenz curve. (b) Mixed native forest with regeneration (Lorenz curve). (c) Plantation forest – all trees planted at same time (line of equality).....29

Figure 6. (a) Bands 5, 4, and 3 composite Landsat-7 image acquired on 2013-09-29 depicting the study area. (b–e) Differences in Ngangao forest areas and (f–i) differences in lowlands (leeward side) with uncorrected and topographically corrected image using Advanced Spaceborne Thermal Emission and Reflection Radiometer (ASTER), Shuttle Radar Topography Mission (SRTM), and TOPO digital elevation models (DEMs).....32

Figure 7. Observed versus predicted aboveground biomass (AGB) (Mg ha^{-1}) values based on individual and combined sensors. In Study II, (a) a single model was used for the whole landscape based on airborne laser scanning (ALS2) data. In Study III, individual and combined sensors were used (b–e) without and (f–i) with land cover stratification (forest/non-forest). The terms ALS, HS, and LTS represent airborne laser scanning data, hyperspectral data, and spectral-temporal metrics based on Landsat time series, respectively. See Table 2 for further details on ALS1 and ALS2.....35

Figure 8. (a) Airborne laser scanning (ALS)-based aboveground biomass (AGB) distribution mapped at a 30-m × 30-m spatial resolution. Histograms were calculated by summing (b) the total area in kilometer square (km^2) and (c) the total AGB in million tons (M tons).....39

Figure 9. (Left) Gini coefficient (GC) map for Yale. (Right) The GC for indigenous and exotic plantations (eucalyptus, cypress, and pine) in the Yale forest in the Taita Hills based on pixel value.....40

Table 1. Field data used in the thesis.....24

Table 2. Characteristics of the airborne laser scanner (ALS) data.....26

Table 3. Characteristics of the hyperspectral (HS) data (Piiroinen 2018).....27

Table 4. Satellite imagery used in the different studies (I, III, and IV).....27

Table 5. Digital elevation models and digital surface model used in different studies (I–IV).....27

Table 6. Summary of recent studies using airborne laser scanning (ALS) for aboveground biomass (AGB) modeling in Africa. 36

Table 7. Summary of recent studies using multispectral satellite images for aboveground biomass (AGB) modeling in Africa.....38

1 Introduction

Global forests play important roles in maintaining the life of creatures on earth, by sequestrating carbon, keeping the hydrological cycle constant, and providing food and shelter for animals and humankind (Bouvet et al., 2018; Houghton 2005; Lewis et al., 2013). Carbon emissions and the loss of ecosystem services from tropical forests as a result of deforestation and degradation are significant. Global forests' carbon stock is estimated to be 861 ± 66 Pg C, with 44% in soil, 42% in live biomass, 8% in deadwood, and 5% in litter (Pan et al., 2011). Tropical forests alone store 471 ± 93 Pg C, of which 56% of carbon is stored in biomass (above and below ground) and 32% in soil, and they emit 2.8 ± 0.5 Pg C $year^{-1}$ through deforestation and degradation (Pan et al., 2011). At present, tropical forests are the source of carbon dioxide emissions rather than sink. Forest variables, such as canopy cover, biomass, and forest structural heterogeneity, among others, can convey the quality of life of animals and humans depending on the forest. For example, if a forest is deforested and degraded, then the habitat of animals is lost or destroyed, water availability via infiltration is low, the local climate becomes warmer, and the emission of carbon because of deforestation triggers climate change. Therefore, mapping and monitoring tropical forests are crucial for social and environmental applications.

African tropical forests are on the verge of destruction because of intensive pressure from land use changes for agricultural expansion (Brink et al., 2014; Pellikka et al., 2013; Pfeifer et al., 2012). The once closed and dense forests have now been converted into mosaic forests surrounded by an agricultural landscape (Sloan and Sayer 2015). In the Afromontane landscape in Africa, carbon stock and biodiversity are not only limited to the mosaic forest, as trees are also common in tropical agro-ecological systems. Vanderhaegen et al., (2015) observed that 80% of total carbon stock was found to be stored in non-forest land uses (agricultural land, home gardens, grazing lands, and teff fields), although indigenous forests store high carbon stock per hectare.

Measuring, mapping, monitoring, and verifying forest biomass effectively and accurately have been some of the largest challenges for countries with the aim of reducing emissions from deforestation and forest degradation (REDD+) under the United Nations Framework Convention on Climate Change (UNFCCC). However, REDD+ ignores the high potential of other land uses for carbon sequestration and excludes trees outside forests, for example in agroforestry and grazing land (Avitabile et al., 2012; Sloan and Sayer 2015; Vanderhaegen et al., 2015). In the Afromontane landscape, the focus should be on reducing emissions from all land uses (REALU) (Vanderhaegen et al., 2015), as the mosaic landscape is comprised of trees outside forests, remnants of forest patches, and young regenerating forests in the tropics (Sloan and Sayer 2015; Zomer et al., 2016).

Forest biomass highly depends on forest structure, tree species composition, topography, and other biotic and abiotic factors (Asner et al., 2009). Small-scale forest biomass mapping and monitoring are more or less based on ground measurements, which are often costly, labor intensive, and time-consuming, and which fail to account for spatial variability as a result of the absence of proper sampling methods. Remote sensing (RS) provides explicit spatial information over large areas, which is impossible using traditional point- and plot-based field measurements. The potential of RS – such as

satellite-, airborne-, and terrestrial-based active and passive sensors – in the estimation of forest variables has been studied intensively, especially in boreal forests (Lutz et al., 2008). However, in the tropics, pan-tropical and continental-scale forest maps are mostly based on coarse-resolution RS data (Avitabile et al., 2016, Baccini et al., 2012, Baccini et al., 2017, Saatchi et al., 2011) that have high uncertainty at the pixel level (Saatchi et al., 2011). Recent higher-resolution maps are restricted to the savannas with relatively low biomass (Bouvet et al., 2018). The accuracy of forest variable estimations obtained using freely available medium- to coarse-resolution RS images has not been adequate for the monitoring and validation of REDD+ and the payment of ecosystem services, among others.

Satellite RS data, for example Landsat, provide wall-to-wall coverage of calibrated surface reflectance with a moderate spatial resolution (30-m optical bands) and temporal resolution (16 days) (Wulder et al., 2012). The open release of Landsat image archives in 2008 has resulted in large-scale mapping, monitoring, and reporting of forests using dense time series at the national, regional, and global scale (Avitabile et al., 2012; Banskota et al., 2014; Brink et al., 2014; Chance et al., 2016; Hansen et al., 2013). The spectral-temporal metrics based on Landsat time series (LTS) data have the potential to improve the accuracy of the prediction models of forest structural attributes through complementary data on the land surface phenology, and they have been gaining attention in the last decade. However, cloud cover severely limits the usability of RS data in the tropics. In most cases, the images can be obtained already preprocessed, excluding the need for further georectification, cloud-masking, or atmospheric correction (Masek et al., 2006; Zhu and Woodcock 2014). However, the topographic effects are typically normalized by end users regionally, and the need for this procedure usually depends on the characteristics of the terrain and on the final application (Reese and Olsson 2011; Vanonckelen et al., 2013; Chance et al., 2016). The spatial resolution of the Landsat images, however, is not sufficient for distinguishing various land covers in the mosaic landscape, and it warrants data fusion with other high-resolution RS images. Furthermore, spectral-temporal metrics based on the LTS are rarely used in the mosaic landscape and in areas frequently covered by clouds and cloud shadows.

Airborne laser scanning (ALS) is increasingly utilized for forestry and environmental applications (Næsset et al., 2016; Valbuena et al., 2016). Such scanning provides a three-dimensional (3D) structure of forest resources that is useful for accurately estimating and mapping various forest inventory variables, for example height, basal area, volume, and biomass (Næsset and Gobakken 2008; Valbuena et al., 2013). Airborne hyperspectral sensor (HS) acquire spatially accurate and spectrally diverse information reflected at narrow wavelengths – from visible to short-wave wavelengths – from forest resources (Piiroinen et al., 2018). However, ALS and HS are relatively expensive per unit area and require high expertise for planning a flight campaign and acquiring, preprocessing, and analyzing data. Furthermore, these data are limited to the landscape and regional scale in few studies; however, the use of small-footprint ALS and HS data are fairly common for upscaling forest structural parameters to the landscape level with the assistance of high- or medium-resolution optical and radar images. The potential of these sensors has not been extensively utilized in the agriculture-forest mosaic landscape, and their limitation in such a landscape is unclear.

Although Landsat is relatively insensitive to forest canopy height (Hudak et al., 2002; Hansen et al., 2016), it would be desirable to integrate ALS, HS, and Landsat data to improve the measurement, mapping, and monitoring of forest structural attributes (Hudak et al., 2002; Phua et al., 2017; Shang et al., 2019). The synergistic use of canopy spectral information from Landsat (TM, ETM+, OLI) and HS images and ALS-based structural information has been successful for modeling biomass (Phua et al., 2017; Vaglio Laurin et al., 2014), canopy height (Hudak et al., 2002), and basal area (Shang et al., 2019), among others. Most of these studies focus on dense tropical forests; however, the integrated use of ALS, HS, and spectral-temporal metrics based on LTS have not been examined in the tropical mosaic landscape and deserve further attention.

The main objective of this thesis was to assess airborne and spaceborne RS techniques for modeling forest structural attributes across a montane forest landscape in the Taita Hills, Kenya. The sub-objectives focused on the effect of topographic normalization on fractional tree cover (Fcover) prediction, the aboveground biomass (AGB), and forest structural heterogeneity modeling using ALS and other RS data and an analysis of the maps of forest structural attributes. Figure 1 summarizes the main content of the thesis and four studies (I–IV).

Study I examined the impact of topography normalization on Fcover modeling in a tropical mosaic landscape. The reference Fcover was based on ALS data. Topographic normalization was carried out by c-correction using three digital elevation models (DEMs) for all available Landsat images between June 2012 and October 2013, several vegetation indices, and spectral-temporal metrics (annual percentiles and means) from the LTS, and it examined whether normalization improves Fcover regressions.

Study II assessesed the determinants for the spatial distribution of an ALS-based AGB using geospatial data and statistical modeling in the tropical mosaic landscape. Plot-level AGBs were estimated using ALS data and a spatial prediction map of the AGB was prepared with an ALS-based multiple linear model. A boosted regression tree (BRT) was used for examining the relationship between the AGB and explanatory variables (the topographical and hydrological, climatic variables and land use classes) at a 250-m × 250-m resolution.

Study III investigated the utility of various RS data sources (simultaneously acquired ALS and HS data and LTS) in predicting the biomass in tropical mosaic landscapes. Furthermore, tests were conducted to determine whether the prior stratification of land cover would improve biomass prediction.

Study IV examined the potential of single ALS and LTS metrics and the fusion of those in modeling forest structural heterogeneity, as described by the Gini coefficient (GC) of tree size inequality in the three forest remnants (Ngangao, Yale, and Vuria). Furthermore, the difference between the three forest remnants and the different forest types were evaluated using the resulting maps of the predicted GC.

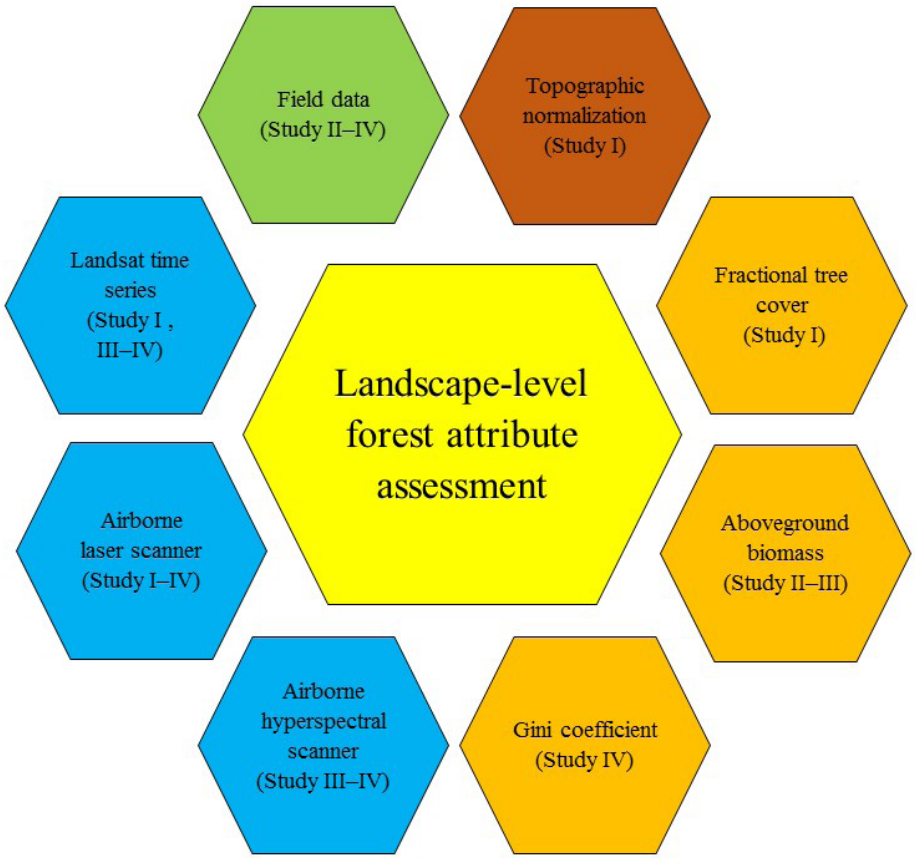

Figure 1. The main contents of the thesis and four studies (I–IV).

2 Background

2.1 Medium-resolution satellite image time series: importance of topographic normalization

With the free availability of medium spatial resolution Landsat imagery, multi-temporal images have been used to fill the gaps created by clouds, cloud shadows, and sensor malfunctioning on target images from reference images (Wulder et al., 2012; Zhu et al., 2019). In other words, a Landsat pixel-based image composite utilizes spectral reflectance pixels that are radiometrically normalized, atmospherically corrected, and screened as cloud-/shadow-free based on an algorithm (Zhu et al., 2015), and it considers the date of observation nearest to the target image (Potapov et al., 2011). It is common practice to calculate spectral-temporal metrics representing spectral reflectance variation in the peak and fall season in areas with less distortion on images as a result of clouds or cloud shadows and sensor failure (Zhu and Liu 2014). In areas with persistent cloud cover and sensor failure, it is only possible to obtain a complete coverage image by using all images acquired throughout the year or two years, or even more (Potapov et al., 2011).

Surface reflectance from the tree cover is affected by various factors, for example atmospheric conditions, clouds, cloud shadows, and haze. In addition, the surrounding terrain casts shadows and has varying illumination effects. Atmospheric correction and the removal of clouds and shadows from optical images are common preprocessing steps; however, the effect of topographic distortion on pixels is not well explored regarding forest change and the LTS (Banskota et al., 2014). In most cases, the images can be obtained already preprocessed, excluding the need for further geo-rectification, cloud-masking, or atmospheric correction (Masek et al., 2006). Figure 2 represents the LTS available for a one-year time period and the spectral-temporal metrics for tasseled cap (TC) transformation (brightness) calculated from it.

Topographic normalization is employed to minimize the effect of shadows and the illumination effects from the terrain. Various topographic normalization algorithms, for example c-correction (Teillet et al., 1982), a sun-canopy-sensor (Gu and Gillespie 1998), and Minnaert correction (Minnaert 1941), are frequently used (Chance et al., 2016; Reese and Olsson 2011; Vanonckelen et al., 2015). Each image in the time series is affected by the topographic effect differently. With regard to studies on the effect of topographic normalization using Landsat pixel-based composites, Chance et al., (2016) found that topographic normalization was not sensitive to forest change detection, and Vanonckelen et al., (2015) observed that topographic normalization has less impact on the accuracy of forest land cover classification. However, in a multi-temporal (two acquisitions) study of the Landsat image, Vanonckelen et al., (2013) observed that the influence of topographic correction is higher than atmospheric correction on land cover classification accuracy.

Multispectral vegetation indices, for example the normalized difference vegetation index (NDVI), become saturated in intact closed-canopy forests (Zhu and Liu 2014). Spectral-temporal metrics provide an opportunity to capture spectral variability during a phenological cycle. The effect of topographic normalization on the spectral-temporal metrics has not been comprehensively addressed, despite recent studies on land cover classification accuracy (Vanonckelen et al., 2013), pixel-based

image composites (Vanonckelen et al., 2015), phenological metrics (Galvão et al., 2016), and forest change detection (Chance et al., 2016). Furthermore, there are relatively few studies demonstrating the effects of terrain illumination on different spectral bands and vegetation indices in tropical forests. In addition, LTS data have rarely been tested in a tropical environment and thus warrant further research.

2.2 Modeling forest structural attributes using multi-source remote sensing data

Tropical forests play a critical role in water balance, biodiversity, species conservation, and the global carbon cycle (IPCC 2000). High-resolution, accurate, and updated forest structure maps in tropical countries are urgently required for the implementation of REDD+, payment of ecosystem services, and other climate change mitigation strategies (Fuller 2006). Monitoring and verification of forest areas and canopy covers are important prerequisites for implementing REDD+, as they convey information regarding forest deforestation and degradation. Furthermore, a detailed forest structure analysis informs one about the productivity of forests, carbon stock, and habitat suitability for wildlife, among other things.

Remote sensing (satellite/airborne) techniques demonstrate potential for forest variable estimation; for example, canopy cover, tree size inequality (the GC), and the AGB have received increasing attention in the last few decades (Higginbottom et al., 2018; Mauya et al., 2015; Næsset et al., 2016). The Fcover is an important indicator for biomass distribution, and information on Fcover is essential for understanding local meteorological processes and hydrological transfers within vegetated environments (Hopkinson and Chasmer 2009; Zhang et al., 2013). Airborne laser scanning has been used for the accurate mapping of forest canopy cover in the boreal forest even without field training data (Korhonen et al., 2013). The GC, based on a Lorenz curve, quantifies tree size inequality among trees within the forest. This coefficient is calculated based on the basal areas (areas occupied by a given diameter at breast height [DBH]) of individual trees (Valbuena et al., 2016). The GC ranges from 0 to 1, where 0

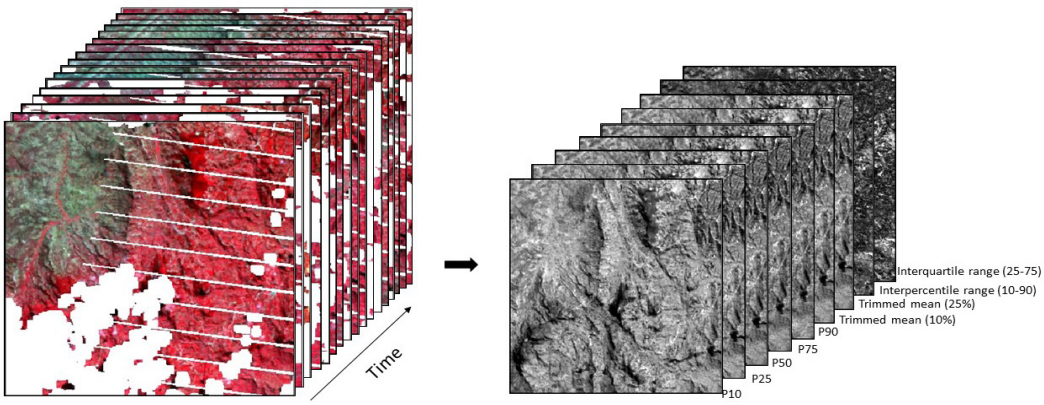

Figure 2. (Left) False color composite of individual Landsat-7 Enhanced Thematic Mapper Plus (ETM+) image available during a one-year time period. The white areas represent clouds and cloud shadows masked from the image, and white lines represent scan line corrector off (SLC-off). (Right) Examples of spectral-temporal metrics (various percentile, trimmed mean, interpercentile, and interquartile ranges) based on tasseled cap transformation (brightness).

represents perfect equality (all trees are of equal size) and 1 represents perfect inequality (a few trees have the largest share) (Nölte et al., 2018).

The accurate quantification of forest AGB and carbon stock is critical for understanding the global carbon cycle. The AGB is estimated in forest inventory plots for each tree using the species-specific allometric equation whenever possible, or the regional model mostly based on the DBH, canopy height, and wood density together is best for estimating the AGB in tropical forests (Chave et al., 2014). In a densely foliated tropical forest, it is common to measure the DBH and wood density and to predict canopy height using species-specific height-diameter allometric equations because of a lack of visibility of the canopy by analog or digital clinometers (Asner et al., 2009; Pellikka et al., 2018). The estimation and spatial variation of the AGB is relatively less frequently studied in African tropical forests (Avitabile et al., 2012) because of political instability, a lack of technical knowhow, difficult accessibility, and less investment in forest management and related studies. Furthermore, the regional estimates of forest structure in tropical forests are highly inaccurate (Houghton 2005). In some countries, forest inventories at the national or local level provide precise and accurate estimates at the plot level; however, for estimates on a large scale, for example at the landscape or country level, the accuracy decreases as a result of environmental variation that is rarely accounted for during extrapolation. Furthermore, coarse spatial resolution RS images, for example a moderate-resolution imaging spectroradiometer (MODIS) and an advanced very high resolution radiometer (AVHRR), are used to predict and extrapolate results that have been based on a limited number of plots scattered across a limited range of site conditions (Baccini et al., 2017).

Airborne laser scanning has been intensively used in boreal and sub-boreal forests with a low AGB density and a homogenous and open forest structure. The applicability of ALS in dense canopy forests and mosaic landscapes has been gaining attention in the last decade. Data from ALS are sufficiently accurate for determining the biomass in different forest types, for example the tropical forests of South America (Clark et al., 2011), Asia (Phua et al., 2017), and Africa (Pellikka et al., 2018). Furthermore, ALS-based statistical models have been used to accurately estimate the forest AGB at a large spatial scale in an African tropical forest (Chen et al., 2015; Næsset et al., 2016; Pellikka et al., 2018; Vaglio Laurin et al., 2014; Vaglio Laurin et al., 2016) and a mangrove forest in coastal wetlands (Fatoyinbo et al., 2018). However, ALS data are expensive to cover the landscape at the national level, especially in the African context; therefore, small-footprint ALS has been employed as an intermediate step for upscaling field-measured AGB to a larger spatial scale (Asner et al., 2012; Vaglio Laurin et al., 2014). However, ALS has not been utilized for identifying tree size heterogeneity in tropical forests, since most of the research is focused on boreal forests (Valbuena et al., 2012; Valbuena et al., 2016). Furthermore, while ALS has been extensively used in the forest context, its use in the agriculture-forest mosaic landscape requires further exploration.

Hyperspectral remote sensing HS data provides detailed spatial and spectral resolution, with the possibility of mapping, inter alia, single species (Piiroinen et al., 2018) and AGB (Vaglio Laurin et al., 2014). However, limited research has been conducted using HS in the agriculture-forest mosaic landscape for predicting AGB.

Medium spatial resolution Landsat images have been widely used for the efficient and timely estimation of the forest AGB in a sub-tropical climatic condition (Dube and Mutanga 2015a; Dube and Mutanga 2015b) and with fractional woody cover (Higginbottom et al., 2018). Landsat images are preferred to others because of their long archive period and consistency in earth observation as well as continuous improvement in the data quality. Landsat provides detailed spectral and textural information and has been a primary source of RS data for resource-constrained regions for mapping forest structural variables. Clouds and cloud shadows can be masked using the function of mask (Fmask) algorithm (Zhu et al., 2015). While most of the studies use single images in the peak or fall season for estimating forest structure, some research explores the use of seasonal time series derived from Landsat images across different seasons and image composites using images available during those time periods (Potapov et al., 2011; Potapov et al., 2012; Zhu and Liu 2014). Seasonal time series and image composites have proven to be better than using single images for estimating the AGB, as multi-temporal datasets are important for distinguishing forest cover (Zhu and Liu 2014) and quantifying forest cover loss and change (Potapov et al., 2011; Potapov et al., 2012), among other things. Furthermore, with seasonal variation persisting in the region, it is assumed that observation based on dense time series of the same pixels can help to discriminate between grassland and forest; this is because during dry seasons, trees better preserve their greenness, whereas the grassland does not.

The combination of ALS data with high-resolution multispectral data improves tree species discrimination at the individual level and supports the accurate estimation of forest attributes. However, no comprehensive studies exist that have fused remotely sensed ALS, HS, and LTS structural and spectral data and vegetation indices to map forest structure and that have analyzed the spatial distribution of forest Fcover, GC, and AGB in Africa.

2.3 Analyzing maps of forest attributes

Spatially explicit mapping of the AGB and GC provides large variation in forest structures at the landscape level. An exploration of local-scale variation of the GC and AGB at the plot-level, as well as between and within forest types, provides an overview of the forest structure in the study area. However, those variations have seldom been explored in tropical indigenous and planted forests, and their extrapolation is rarely done at the landscape level in the absence of high-resolution RS data. High-resolution mapping of forest structural attributes further provides opportunities to understand their distribution in remote regions; this would otherwise be impossible in logistically difficult areas. Furthermore, quantification and knowledge about the spatial distribution of forest structure attributes improve decision making regarding timber, wood products and fuelwood extractions, and sustainable forest management (Fuller 2006). Decisions based on ground-based forest inventories, which are not uniformly distributed over the forest areas, will lead to incorrect conclusions.

Forest structural attributes, such as the AGB, can vary specifically because of basal area, density of trees with a higher diameter, soil, height, site index, and canopy vertical profiles, among other things (Asner et al., 2009; Cuni-Sanchez et al., 2017; Gourlet-Fleury et al., 2011; Holl and Zahawi 2014; Loubota Panzou et al., 2018). Those structural attributes are determined

by environmental and biotic controls in the landscape; for example, trees positioned on the windward side of the topography receive more precipitation and solar radiation – i.e., the environment is more favorable for growth, compared to the leeward side (Asner et al., 2009). The causes of change in the biomass can be the anthropogenic and/or indirect impacts of climate change. However, the reasons for the spatial distribution of biomass can be different across continents. However, to understand the spatial distribution of forest structural attributes, plot-level data are not sufficient, and spatially explicit maps are required, which provide an overview at the landscape level.

3 Material and methods

3.1 Study area

This thesis was conducted in the Taita Hills, which are located in southeastern Kenya (3° 25' S, 38° 20' E) and are part of the northernmost portion of the Eastern-Arc mountain (EAM) range with high conservation value (Lovett and Wasser 1993) (Figure 3). The Afromontane forests are particularly valuable in terms of biodiversity, other ecosystem services, and carbon stock (Cuni-Sanchez et al., 2017, Vanderhaegen et al., 2015). The Taita Hills rise abruptly from the semi-arid Tsavo plains at 600–700 m to a series of ridges reaching 2,208 m at the Vuria peak (Aerts et al., 2011).

Given the orographic rainfall pattern, the southeastern slopes receive more precipitation, while the northwestern slope in the rain-shadow receives less precipitation (Pellikka et al., 2009). The study area has a bimodal rainfall pattern, with long rains between March and May and short rains between November and December (Pellikka et al., 2009). As a result of the altitude difference, the hills experience a lower mean annual temperature (18.2 °C) compared to the lowlands (24.6 °C).

The remnant montane forests can be separated into lower and upper montane forests. The lower parts are taller and drier, compared with the elfin forest-like upper parts, which receive significant amounts of precipitation through a mist. These mist forests on the top of Vuria typically have only one layer and are covered by epiphytic mosses and lichens (Enroth et al., 2013, Stam et al., 2017).

The landscape is a highly fragmented mosaic of montane forest patches, exotic plantations, and agriculture, with agroforestry and horticulture being common (Aerts et al., 2011). Some of the most common native species observed in the field include *Tabernaemontana stapfiana, Macaranga capensis, Oxyanthus speciosus, Phoenix reclinata,* and *Celtis africana*. Otherwise, the landscape consists of smallholder

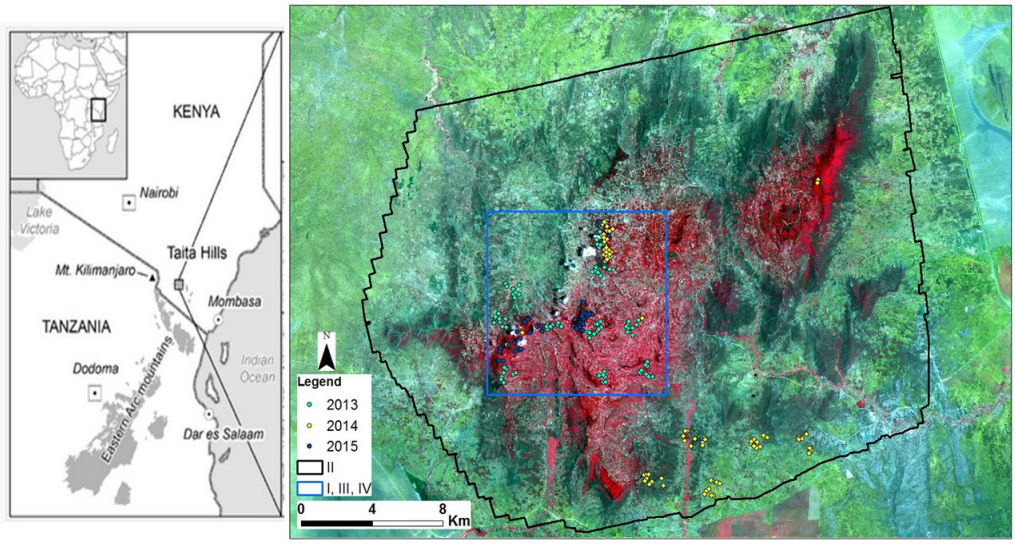

Figure 3. Location of the Taita Hills study area with Sentinel-2A multi spectral instrument satellite image from 8 October, 2016 in the background. The area covered by the blue box represents airborne laser scanning (ALS1) and hyperspectral image coverage (10,000 ha), and the black box represents ALS2 coverage (~55,000 ha). See additional details about ALS (1 and 2) in Table 2.

Table 1. Field data used in the thesis

Year (Months)	Number of plots	Coverage	Study
2013 (January–February)*	91	Lowland	II, III
2014 (January–February)*	86	Lowland and forest	II, III, IV
2015 (October)**	48	Forest	II, IV

* Collected by other participants
** Author personally planned and executed the field campaign

agriculture (mainly maize fields), plantations of exotic trees (*Eucalyptus spp., Pinus patula*, *Cupressus lusitanica* and *Acacia mearnsii*), bushland, and settlements (Figure 1). Rocky and sandy areas outside the forests are dominated by *Acacia mearnsii*, while typical agroforestry species are *Grevillea robusta* on the hills and *Persea Americana* and *Mangifera indica* in the lowlands (Thijs et al., 2014, Thijs et al., 2015).

The Taita Hills in Kenya were chosen because of their extensive forest inventories as well as large-scale HS (10,000 ha) and multi-temporal ALS coverage (10,000 ha and ~ 55,000 ha) as part of the BIODEV[1] and CHIESA[2] projects. Furthermore, the study area is a miniature version of Kenya and East Africa, representing a broad range of forest types and different land covers, from savannas and grasslands in lowland areas to evergreen indigenous and exotic forests in montane forests on the hilltops.

3.2 Field data

Field sample plots data were used in this thesis for modeling and predicting the AGB (Studies II–III) and tree structure (Study IV). The sampling design of the Land Degradation Surveillance Framework (LDSF) (Vågen et al., 2015), with slight modification, was used for field measurements (Heiskanen et al., 2013). The forest inventories were carried out in a total of 225 circular 0.1-ha plots (radius 17.84 m) in 2013–2015 (January–February in 2013 and 2014 and October in 2015), across the whole span of the Taita Hills (Table 1). In 2013 and 2014, 177 plots were randomly sampled within 10-km × 10-km (100 ha) (blue box in Figure 3) clusters in the hills and lowlands. In addition, in 2015, 48 plots were subjectively sampled in the high biomass forest areas, especially on the hills. Plot selection was guided by visible to near infrared imaging spectroscopy data (AisaEAGLE) (Piiroinen et al., 2015) and ALS data (Heiskanen et al., 2015) acquired in February 2013 to cover variation in the composition and canopy structure of tree species.

In the plots, for all tree stems with a DBH ≥ 10 cm, the DBH was measured (Marshall et al., 2012) at 1.3 m or above basal irregularities such as buttresses, and tree species were identified in full (genus and species) by a local para-taxonomist. Moreover, tree height (H) was measured for at least three sample trees (minimum, median, and maximum DBH > 10 cm) in the forest plots (0.1 ha) and at least one median tree (DBH < 10 cm) in each 0.01 ha using a laser range finder or hypsometer (Laser Technology TruPulse 360, Suunto hypsometer). In the lowlands, H was measured for the majority of trees, but only a few trees (i.e., trees with a minimum, maximum, and median DBH) were measured inside the forests because of low visibility of the crown. Furthermore, in the 0.1-

1 https://www.worldagroforestry.org/project/biocarbon-and-rural-development-biodev

2 http://chiesa.icipe.org/

ha plot, for palms with a DBH > 10 cm, height (in m) and DBH (in cm) were measured, and the number of stems were counted.

The sample plot centers were positioned using the Trimble GeoXH GNSS receiver, and differential correction was made using the GNSS base station located in Wundanyi town (Taita Research Station). In 2013 and 2014, slope corrections for field sample plots were performed afterward based on the digital terrain model (DTM) derived from ALS (acquired in February 2013). In 2015, slope corrections were done in the field.

Field-based tree height estimations were difficult, especially in closed-canopy forests. Tree height imputations were done separately for trees in forests and lowlands to evaluate the possible advantages of stratification. Non-linear mixed-effect modeling and plots as random effects (e.g. Mehtätalo et al., 2015) were employed to calibrate the H-D model for each sample plot. The 'nlme' package (Pinheiro et al., 2014) in R statistical software was used to fit the models. Table 1 presents overview of the field data. The general workflow of these data in Studies I–IV is illustrated in Figure 4.

3.3 Remote sensing datasets

3.3.1 Airborne laser scanning (ALS) data

The discrete-return airborne laser scanning data (ALS1) were acquired on 4–5 February, 2013 for the 10-km × 10-km area (hereafter Sentinel site), and ALS2 data were acquired on January 26 and February 6 and 8, 2014 and on February 5, 6, 11, and 13, 2015 for the whole span of the Taita Hills (Table 2). Airborne laser scanning -ALS1 was used in Studies I, III, and IV, and ALS2 was used in Studies II and IV. The ALS points were classified as ground or non-ground using LAStools (Isenburg 2014). The ALS ground points were subsequently used to construct a 2-m bare-earth DTM. The ALS point cloud elevation was normalized using the DTM from the corresponding campaign to obtain the aboveground height. An area-based approach was used by aggregating point clouds in the forest inventory field sample plot for describing canopy height and canopy density metrics (Næsset 2002). The ALS point clouds were clipped to the extent of each forest inventory field sample plot. Furthermore, ALS metrics describing the forest structure were extracted for each field sample plot (Study II–IV) from the corresponding clipped ALS normalized point clouds using Fusion software (McGaughey 2016). In Study I, the all-echo cover index (ACI) (e.g. Morsdorf et al., 2006) was calculated as a proxy of the canopy gap fraction (Fcover) for 2,000 randomly selected points in the Sentinel site. At each random point, the Fcover was estimated for a 90-m × 90-m area corresponding to a 3 × 3 pixel window of Landsat images.

3.3.2 Hyperspectral sensor (HS) data

Hyperspectral data (visible to NIR bands, 400–1,000 nm [bandwidth 4.5–5.0 nm]) were acquired using airborne AisaEAGLE sensors (Specim, Spectral Imaging Ltd., Finland) on 3–8 February, 2013 (Piiroinen et al., 2018). AisaEAGLE is a pushbroom scanner with an instantaneous field of view of 0.648 mrad and a field of view of 36.04° (Table 3). The sensor produced 129 bands with an output pixel resolution of 1 m. HS was used for predicting the AGB (Study III) and mapping the forest boundary (Study IV).

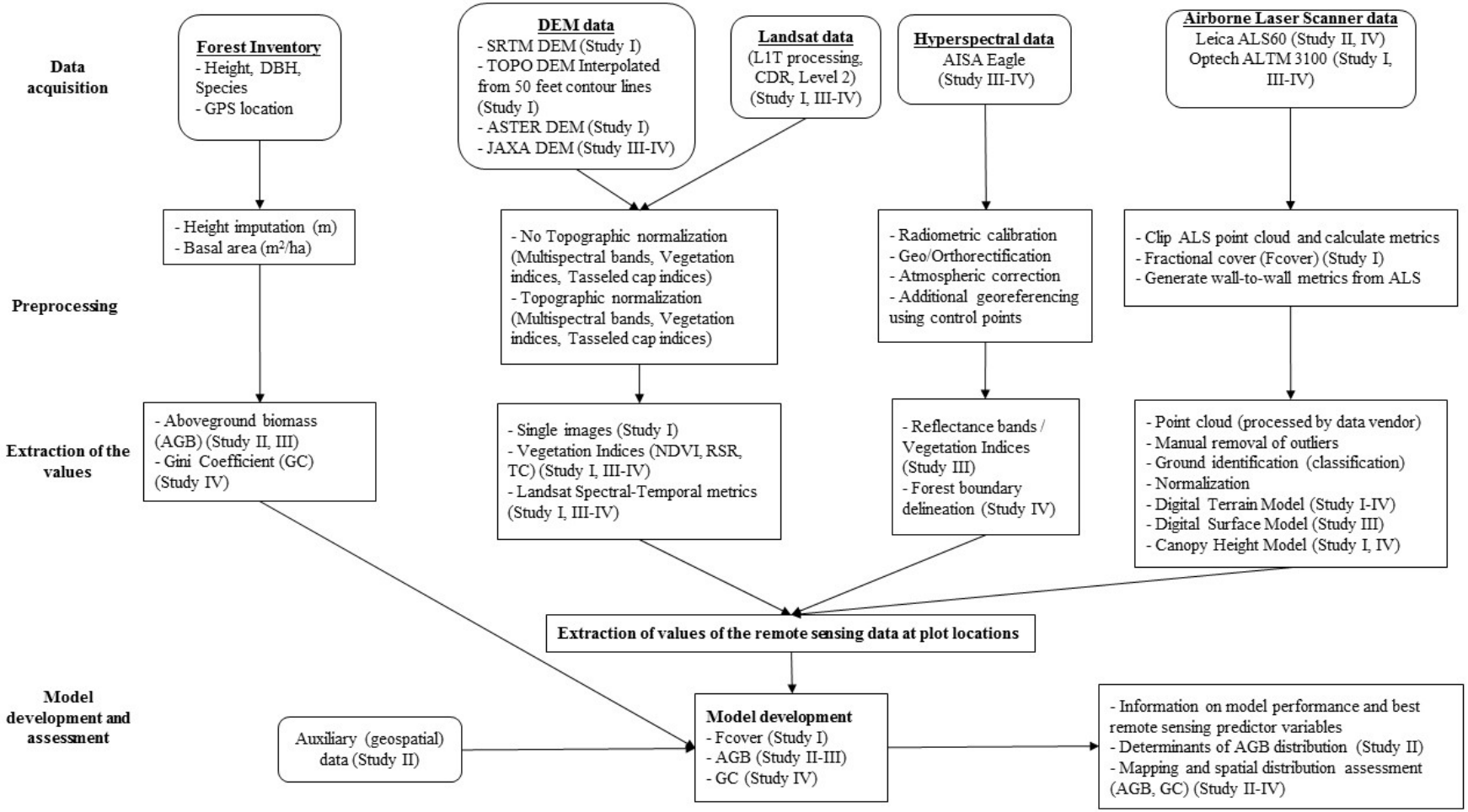

Figure 4. Overview of the methodology.

Table 2. Characteristics of the airborne laser scanner (ALS) data.

Parameter	ALS1	ALS2
Date of acquisition	2013	2014 and 2015
Sensor	Optech ALTM 3100	Leica ALS60
Mean flying height above ground (m)	760	1,460
Pulse rate (kHz)	100	58
Scan rate (Hz)	36	66
Maximum scan angle (degrees)	±16	±16
Mean pulse density (pulses m^{-2})	9.6	3.1
Mean return density (returns m^{-2})	11.4	3.4
Maximum number of returns per pulse	4	4
Mean footprint diameter (cm)	23	32

3.3.3 Multispectral spaceborne (MS) data

All available Landsat surface reflectance images were downloaded from the USGS Earth Resources Observations and Science (EROS) Center archive with an L1T processing level for the period between June 2012 and April 2015 (Table 4). The climate data record (CDR) and level-2 images were atmospherically corrected, radiometrically calibrated, and orthorectified using ground control points and DEM data to correct for relief displacement (Zhu and Woodcock 2014; Zhu et al., 2019). Moreover, clouds and cloud shadows were detected using an Fmask algorithm (Zhu et al., 2015). The following were used for further analysis: blue (0.45–0.52 μm), green (0.52–0.60 μm), red (0.63–0.69 μm), near-infrared (NIR) (0.77–0.90 μm), shortwave infrared (SWIR) 1 (1.55–1.75 μm), and SWIR 2 (2.09–2.35 μm) from the ETM+ and blue (0.45–0.51 μm), green (0.53–0.59 μm), red (0.64–0.67 μm), NIR (0.85–0.88 μm), SWIR 1 (1.57–1.65 μm), and SWIR 2 (2.11–2.29 μm) from the OLI.

3.3.4 Digital elevation models (DEMs) and digital surface model (DSM)

Six sources of DEMs and one source of a DSM were tested for topographic normalization and height normalization (Table 5). Three of the DEMs, namely the Shuttle Radar Topography Mission (SRTM) DEM (SRTM 2014), the Advanced Spaceborne Thermal Emission and Reflection Radiometer (ASTER) (Jspacesystem 2011), and the Japan Aerospace Exploration Agency (JAXA) (JAXA 2015), provide almost global coverage, while the ALS1 DEM and ALS1 DSM provide coverage of the Sentinel site in the Taita Hills, and the TOPO DEM is based on scanned topographic maps of a 1:50,000 scale of the Survey of Kenya (Pellikka et al., 2013). The ALS2 DEM provides coverage of the whole span of the Taita Hills. If a different projection was observed, then all DEMs and DSMs used in all studies were projected to the Universal Transverse Mercator 37 S WGS 84.

Table 3. Characteristics of the hyperspectral (HS) data (Piiroinen 2018).

Parameter	Value
Numerical aperture	F/2.4
Spectral range	400–1,000 nm
FWHM	3.3 nm (max)
Spectral binning options	1, 2, 4, 8
Spectral sampling rate (bin 8)	8.64–9.55 nm
Number of bands	64–488
Field of view	37.7 degree (with FODIS)
Spatial pixels	1,024 (total)
Radiometric resolution	12 bits
Frame rate, up to (frames/s)	30–160 (bin 1–8)

Table 4. Satellite imagery used in the different studies (I, III, and IV).

Imagery	Number and period	Data quality	Path/Row
Landsat ETM+ and OLI (Study I)	17 + 4 (June 2012 to October 2013)	Climate Data Record data	163/062
Landsat OLI (Studies III, IV)	42 (April 2013 to April 2015)	Landsat collection 1 Level-2	163/062

Table 5. Digital elevation models and digital surface model used in different studies (I–IV).

Digital elevation model	Original resolution and projection	Resolution and projection used in study	Study
ALS 1 DEM, ALS 1 DSM	2 m (Universal Transverse Mercator 37 South; Horizontal Datum: WGS 84)	2 m and 5 m	I, III–IV
ALS 2 DEM	2 m (Universal Transverse Mercator 37 South; Horizontal Datum: WGS 84)	2 m	II, IV
SRTM	1 arc-second (~30 meters) (Projection: Geographic; Horizontal Datum: WGS 84)	30 m	I
ASTER	1 arc-second (~30 meters) (Projection: Geographic; Horizontal Datum: WGS 84)	30 m	I
JAXA	1 arc-second (~30 meters)	30 m	III–IV
TOPO	20 m (transverse Mercator projection with a Clarke 1880 spheroid and an Arc 1960 datum and a planimetric accuracy of 50 m with an altimetric accuracy of 8 m) (Clark and Pellikka 2009)	30 m	I

3.3.5 Auxiliary data

The spatial patterns of AGB distribution were examined with the help of auxiliary environmental data (Study II). This included climatic variables (mean annual temperature [MAT] in °C and mean annual precipitation [MAP] in mm); topographical and hydrological variables (ALS2-based DEM, slope, aspect, topographic position index [TPI], topographic wetness index [TWI], rivers, and soil); and land use classes (cropland, plantation, building, and road).

3.4 Preprocessing and image compositing

The Taita Hills have a mountainous topography. Hence, spectral bands (blue, green, red, NIR, SWIR1, and SWIR2) of all available Landsat-7 ETM+ images between June 2012 and October 2013 (Study I) and Landsat-8 OLI images between April 2013 and April 2015 (Study III–IV) were topographically normalized (removing topographic shadows and varying illumination caused by terrain). The semi-empirical c-correction method (Teillet et al., 1982) was used with the SRTM DEM, ASTER DEM, and TOPO DEM (Study I) and the JAXA DEM (Studies III–IV) (see section 3.3.4).

The vegetation indices, for example TC indices (brightness, greenness, wetness) (Crist 1985), were calculated using the topographically corrected surface reflectance (Studies I and III–IV). The NDVI (Rouse et al., 1973) and reduced simple ratio (RSR) (Brown et al., 2000) were calculated using the non-corrected surface reflectance, as they were found to be robust against topographic effects (Studies I and III–IV).

Landsat spectral-temporal metrics based on images available during the above-mentioned time periods provide an opportunity for the production of surface reflectance images devoid of clouds, cloud shadows, or haze. The spectral-temporal metrics were computed based on the statistical distribution of annual vegetation index values and bands to provide complete, cloud-free coverage of the study area (Potapov et al., 2012). All available Landsat-7 ETM+ time series images (June 2012 to October 2013) were used in Study I, and Landsat-8 OLI time series images (April 2013 to April 2015) were used in Studies III–IV. The spectral-temporal metrics included several percentile values (10%, 25%, 50%, 75%, and 90%), the trimmed mean (10% and 25%), the inter-percentile range (10–90), and the interquartile range (25–75) for all five vegetation indices (i.e., NDVI, RSR, and TC indices) and Landsat spectral bands. Those metrics were computed for each pixel using all cloud-free observations with reflectance data. The spectral-temporal metrics based on vegetation indices were used in Study I, and vegetation indices and bands were used in Studies III and IV.

3.5 Modeling

Field sample plots' AGB and GC data were derived from forest inventories carried out in the years 2013–2015. Chave et al., (2014) pan-tropical allometric equation that derives AGB as a function of DBH, imputed height, and wood density was used as the main allometric equation to estimate the AGB at each field sample plot. Species-specific allometric equations for AGB estimation were used when possible for plantation forests, Acacia mearnsii and Eucalyptus spp. (Paul et al., 2013), Pinus spp. (Henry et al., 2011), and Phoenix reclinata (Brown 1997). The GC, which represents tree size inequality, was calculated based on basal area distribution in the field plot (Figure 5). The GC ranges from 0 to

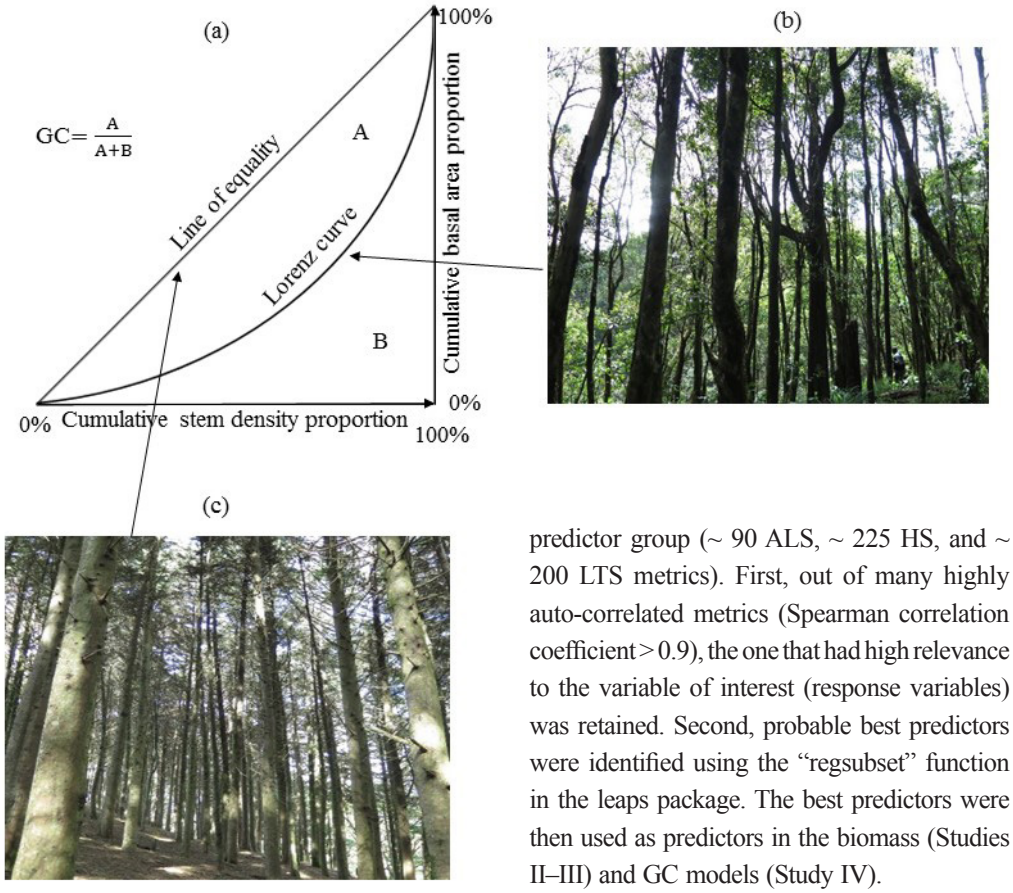

Figure 5. (a) Relationship between the Gini coefficient (GC) and the Lorenz curve. (b) Mixed native forest with regeneration (Lorenz curve). (c) Plantation forest – all trees planted at same time (line of equality).

1, where 0 represents perfect equality (all trees of equal size) and 1 represents perfect inequality (few trees have the largest share) (Nölte et al., 2018). Figure 5 illustrates that a plantation forest has even-sized distributions, while an indigenous forest has bimodal diameter distributions.

Forest structure attributes were modeled from single or fused ALS, HS, and LTS data to understand the ability of the dataset to estimate the Fcover, AGB, and GC in tropical mountains and to assess the usefulness of the integration of those data. A two-step predictor variable selection strategy was employed because of the large number of predictor variables within each predictor group (~ 90 ALS, ~ 225 HS, and ~ 200 LTS metrics). First, out of many highly auto-correlated metrics (Spearman correlation coefficient > 0.9), the one that had high relevance to the variable of interest (response variables) was retained. Second, probable best predictors were identified using the "regsubset" function in the leaps package. The best predictors were then used as predictors in the biomass (Studies II–III) and GC models (Study IV).

Predictive models were developed between the ALS-based, HS-based, and LTS-based metrics as independent variables (individually or fused) and the field sample plots (tree inventory data – AGB [Studies II–III] and GC [Study IV]) as response or dependent variables. Also, spatially continuous ALS-, HS-, and LTS-based metrics were created (the same metrics that were calculated for the clipped plot and selected in the final model) for the entire area of interest. The predictive equations developed were then applied to the entire area of interest to produce spatially explicit estimates (30-m × 30-m grid size) of inventory attributes (AGB [Studies II–III] and GC [Study IV]). In Study II, determinants for the spatial patterns of the AGB were modeled using BRTs.

3.6 Statistical analysis

In Study I, a simple linear regression was used to model the relationships between the Fcover and different predictors with and without topographic normalization. The model was trained with 2,000 random plots extracted from fractional cover metrics from ALS data covering the representative site with vegetation variability at the landscape level. The model fit was evaluated based on the root mean square error (RMSE) and coefficient of determination (R^2). In Study II, a simple linear regression-based model was used to produce the spatial prediction of the AGB, and BRTs were used to examine the relationship between the predicted AGB and the explanatory variables. The model fit was assessed using the total explained deviance of the BRT model. In Study III, a linear regression was used for the AGB modeling. Furthermore, an accuracy assessment was based on leave-one-out cross validation (LOOCV) RMSE, relative LOOCV RMSE, and pseudo and cross-validated coefficients of determination (R^2), and the hypothesis test was based on intercept (a) and slope (b) of the linear regression (H0: a = 0, H0: b = 1) and the ratio of the sum of square (SSR). In Study IV, a beta regression was used to model and predict the GC based on ALS metrics and Landsat spectral temporal metrics. Beta regression models were constructed using different combinations of metrics (ALS1, ALS2, LTS, ALS1+LTS, and ALS2+LTS). Those models were assessed by LOOCV to safeguard against possible over-fitting. All models were evaluated by comparing their accuracy (relative mean difference, RMSE) and relative RMSE, the cross-validated R^2, a hypothesis test, and SSR. It was anticipated that changes in the composition and forest inventory of the tree species in the field sample plots were small and over 2–3 years, as no sample plots were harvested during this period. See more explanation about these equations in Study I–IV.

4 Results and discussion

4.1 Effect of topographic normalization

The effect of topographic normalization on Fcover modeling was evaluated in the tropical mountain landscape. Reflectance bands from single-date images, the vegetation indices, and the spectral-temporal metrics (annual percentile and means) from the LTS were calculated and examined to determine whether normalization improved Fcover regression. Furthermore, a comparison between global (SRTM and ASTER) and regional (TOPO) DEMs was performed. The reference Fcover was calculated from ALS1.

The cosine of the solar incidence angle (cos[i]) was calculated from each DEM, and in the regression analysis between cos(i) and reflectance bands without topographic normalization, cos(i) based on the SRTM DEM demonstrated the strongest relationship (the highest R^2 values) with reflectance in all bands throughout the seasons. Furthermore, cos(i) based on the TOPO DEM displayed the weakest relationship with reflectance bands (Figure 6, Study I). The results are in line with the general preference of a three arc sec SRTM DEM over an ASTER DEM (Frey and Paul 2012; Hirt et al., 2010). The vertical accuracy of SRTM is better than the ASTER DEM; this is proved by higher correlation (R^2 = 0.999 and RMSE = 4.68) between the SRTM DEM and the LiDAR-based DSM (Figure 5, Study I), which is in line with Elkhrachy (2018).

Furthermore, in the regression analysis between the SRTM-derived cos(i) and vegetation indices, the strongest relationship was observed between cos(i) and brightness, greenness, and wetness, while the lowest relationship was observed between the NDVI and the RSR (Fig, 7, Study I). The low sensitivity of the NDVI and RSR to topographic variations could be explained, as they are effectively a ratio of some reflectance bands and compensate for the variations in illumination of the scene. Galvão et al., (2016) also observed that the NDVI was less sensitive to seasonal changes in the biophysical attributes, and Song and Woodcock (2003) found that the NDVI is unaffected by topographic effects over a great range of sun elevation angles. The results are in contrast to those by Song and Woodcock (2003) in regard to the TC indices. Not only are the topographic effects, as measured by the strength of the relationship between cos(i) and reflectance, the most prominent from the middle of May to late September (DOY 136–270), but they also increase towards the end of the year (Figs. 6 and 7, Study I). This is explained by the low sun elevation angle in the study area during those periods. Figure 6 illustrates the difference between a Landsat-7 image topographically corrected with the ASTER, SRTM, and TOPO DEMs and uncorrected in the forest and lowlands areas.

The spectral-temporal metrics were calculated separately for reflectance data (no topographic normalization) and the topographically normalized reflectance data using the SRTM DEM. In general, the Fcover was best predicted (the highest R^2 values) during the dry season (July–September) when observed for a single-date Landsat image. The strongest linear relationships were observed for the RSR and brightness, while the weakest were observed for greenness. The spectral-temporal metrics exhibited similar patterns to single-date images, with improvement in R^2 values for TC indices but no effect for the NDVI and RSR when topographic normalization was performed. The improvement was the greatest for brightness. In general, the strongest relationships were provided by the lower percentile values, particularly 10% and 25% percentiles and the trimmed mean (10%). These correspond to the lowest annual values of the vegetation indices.

In this study, an ALS1-based Fcover proxy was used, which other researchers have found to be a fairly accurate estimate of forest canopy cover (Korhonen et al., 2013; Heiskanen et al., 2015). Large samples of Fcover were available in areas representing diverse topographic conditions, which would otherwise be impossible based on a field visit. We opted to normalize sun-terrain-sensor rather than sun-canopy-sensor topographic effects (Gu and Gillespie 1998), as the sample plots were randomly selected from the agriculture-forest mosaic landscape. We used spectral-temporal metrics based on a statistical distribution of the vegetation index values (e.g., Potapov et al., 2012) instead of single, cloud-free images or selection of the best annual pixel based on compositing rules (e.g., White et al., 2014). Similar results were obtained, since topographic normalization did not improve forest cover and change detection based on pixel-based image composites (Chance et al., 2016; Vanonckelen et al., 2015). The lower percentile spectral-temporal metrics representing dry season conditions were best for the prediction of Fcover. Furthermore, Galvão et al., (2016) have found NDVI-based phenological metrics to be sensitive to topography in seasonal, deciduous forests in the low-altitude, mountainous area in southern Brazil. The results, however, are not directly comparable, because of a difference in the sensors used, the forest types, and latitude. Further studies should thus examine how topographic effects on seasonal metrics depend on latitude.

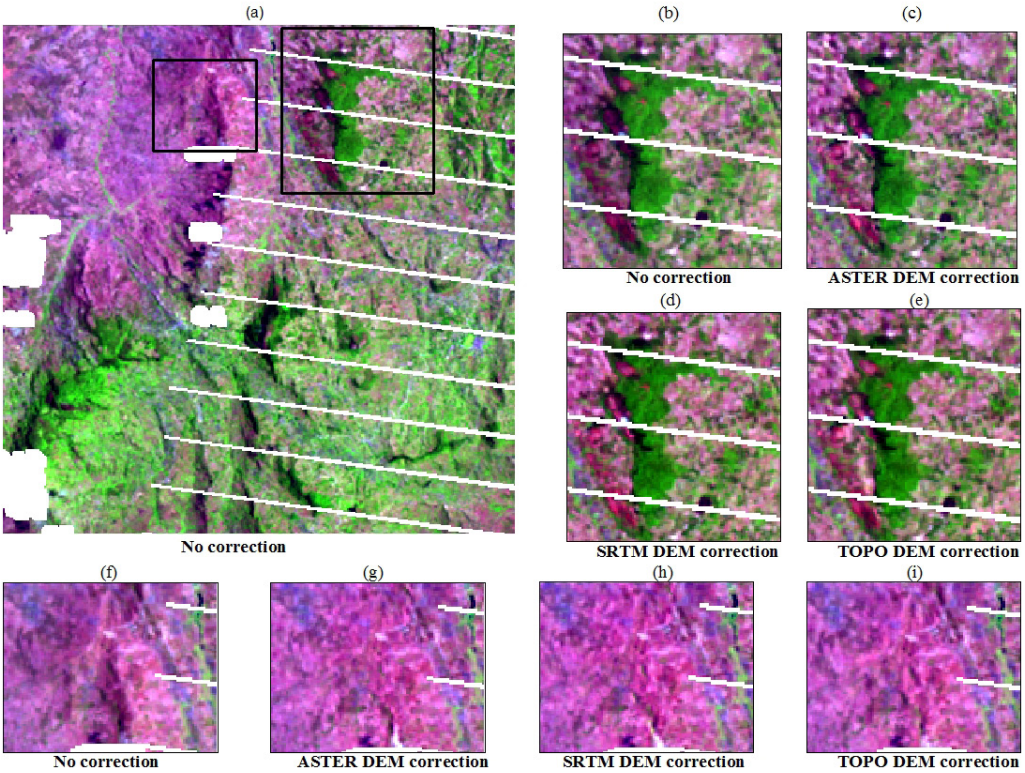

Figure 6. (a) Bands 5, 4, and 3 composite Landsat-7 image acquired on 2013-09-29 depicting the study area. (b–e) Differences in Ngangao forest areas and (f–i) differences in lowlands (leeward side) with uncorrected and topographically corrected image using Advanced Spaceborne Thermal Emission and Reflection Radiometer (ASTER), Shuttle Radar Topography Mission (SRTM), and TOPO digital elevation models (DEMs).

The topographic normalization slightly deteriorated the model fit in the case of the NDVI and RSR, suggesting that normalization may add noise to the data and that topographic normalization should be avoided in cases of vegetation indices if the final goal is to predict tree cover. Persistent clouds and cloud shadows, as well as the sensor malfunction (SLC-off) in Landsat 7, results in fewer sample plots during wet seasons. Further research should examine whether spectral-temporal metrics based on Landsat images during dry seasons only could yield different results, rather than using all images available throughout the year.

4.2 Prediction of forest structure attributes at landscape scale: benefits of data fusion

Airborne laser scanning provided the most accurate RS data for the predictive modeling of live, woody AGB in the tropical mosaic landscape. Parametric models were able to model the AGB with higher accuracy and without any signs of systematic over- or under-estimation in any range of the values. The relationship between square-root-transformed AGB and ALS-based metrics was linear. Furthermore, the analysis in Studies II and III were performed across tropical mosaic landscapes covering the whole span of the Taita Hills and a subset thereof (Sentinel area), respectively. In Study II, the best AGB model was fitted with an R^2 of 0.88 and an RMSE of 52.9 Mg ha^{-1} based on the canopy height metrics (25^{th} percentile of height values) and canopy cover metrics (percentage of all returns above 3 m divided by the total first returns) from the ALS2 data. In Study III, the ALS1 data alone provide robust models for AGB mapping ($RMSE_{CV}$ 51.5 Mg ha^{-1} [42.7%] and R^2 0.90) based on canopy cover and density (percentage of all returns above 3 m) and canopy height (25^{th} percentile of the first return heights) without stratification. The results were back-transformed (squared), and the square of the residual standard error was added to the predicted values. Table 6 presents a summary of AGB estimations in various ecosystems with ALS data, and Table 7 with multispectral images in Africa.

Studies II and III used varying pulse densities, and the accuracy of the biomass prediction models were similar, indicating that a high pulse density is not required for the estimation of aboveground forest biomass. In other literature, different height bins derived from ALS point clouds (Vaglio Laurin et al., 2016) and mean canopy profile height (Asner et al., 2011; Asner et al., 2012), among others, are used as predictors for the AGB in a tropical forest. The accuracy of the AGB estimates obtained in Studies II and III were higher than most of the ALS-based studies conducted in Africa. In Study III, the accuracy did not improve for the ALS-based model when the land cover was stratified. The inclusion of land cover in the AGB prediction models does not always improve accuracy; in Avitabile et al., (2012), it led to biomass overestimation for partially deforested areas, as the errors and limitation in the land cover map were propagated in the AGB map. However, this was not the case in Study III, since we used canopy height model and field information in determining forest and non-forest classes. Overall, it was observed that ALS performed comparatively better in the landscape mosaic (Asner et al., 2012; Pellikka et al., 2018) and mangrove forest (Fatoyinbo et al., 2018) than in woodlands (Egberth et al., 2017; Ene et al., 2016 ; Mauya et al., 2015; Næsset et al., 2016) and moist evergreen (Vaglio Laurin et al., 2014;Vaglio Laurin et al., 2016) and tropical moist forests (Asner et al., 2011). Furthermore, small-footprint discrete return ALS data are commonly used in other studies; however, in Studies II and III, ALS data were acquired for whole the landscape.

Hyperspectral sensor bands and derived vegetation indices had limited predictive power when used alone in the AGB model. The stratified models based on HS predicted AGB with higher accuracy ($rRMSE_{CV}$ 60.2%, R^2 0.79) compared to non-stratified models ($rRMSE_{CV}$ 74.4%, R^2 0.69). Moreover, HS data performed poorly in AGB models for the forest plots ($rRMSE_{CV}$ 39.1%, R^2 0.21) and non-forest plots ($rRMSE_{CV}$ 87.6%, R^2 0.45). Despite variations in spectral responses, HS-based AGB models did not performed well. This can explain why AGB estimation cannot be based solely on HS-based metrics. Instead, further studies should expand, inter alia, the number of metrics, vegetation indices, original reflectance bands, and MNF transformation and endmember fractions obtained from linear spectral mixture analysis.

The spectral-temporal metrics based on the LTS were used to predict the AGB in the heterogeneous landscape mosaic (Study III). The stratified models based on the LTS predicted AGB with higher accuracy ($rRMSE_{CV}$ 58.6%, R^2 0.81) compared to non-stratified models ($rRMSE_{CV}$ 70.5%, R^2 0.72). In contrast, the LTS models were poor for forest ($rRMSE_{CV}$ 37.5%, R^2 0.26) and non-forest ($rRMSE_{CV}$ 95.6%, R^2 0.35) classes.

In Study III, ALS-based metrics had greater utility than HS and LTS-based metrics in predicting AGB when used alone. Estimating AGB with ALS and HS metrics yielded slightly better predictions (lower $rRMSE_{CV}$ 40.5% and higher R^2 0.91). This improvement indicates possible synergies between the two data sets, similarly to Vaglio Laurin et al., (2014). In addition, the modeling accuracy improved considerably when the land covers were stratified as forest and non-forest classes (RMSE 33.1 % and R^2 0.94). Furthermore, the combination of ALS with LTS data resulted in minor improvements in the forest and non-forest plots. However, significant improvements have been reported on the synergistic use of Landsat-based texture variables and ALS data in tropical rainforests in studies outside Africa (Phua et al., 2017). The spectral signature of the dense vegetation becomes saturated in closed-canopy forests; therefore, further studies should consider using texture measures, as the capability of spatial resolution can be enhanced in AGB detection (Phua et al., 2017). In the Miombo woodlands, Egberth et al., (2017) observed that the rRMSEcv decreased from 66.2% (using a Landsat-8 image alone) and 50.3% (using ALS data alone) to 49% for the combination of Landsat-8 and ALS data; this is still a comparatively higher error compared to Study III ($rRMSE_{CV}$ 40.1% and R^2 0.91). It clearly demonstrates the benefit of using spectral-temporal metrics based on Landsat image time series compared to a single image. Further conclusions could be drawn, as the LTS is better for a mosaic landscape.

Figure 7 presents the scatterplots of the observed values plotted against predicted values for AGB (Mg ha^{-1}) obtained by LOOCV at the plot level in Studies II and III for different sensor combinations. A simple linear regression model was able to capture the linear relationship between structural and spectral data from ALS, HS, and LTS and AGB. The spatial resolution of Landsat is compatible with the plot size, and there was no overfitting in the model.

In Study II, the ALS-based AGB map was predicted at a 30-m × 30-m resolution based on the best-fitting multiple linear regression. The map displays the quantity and spatial variation of the AGB across the studied agriculture-forest landscape mosaic. The largest values were concentrated on the montane forest patches on the hills and slopes with northeastern and southeastern aspects. In general, the AGB density decreases towards the lower elevations. Furthermore, lower densities (less than 30 Mg ha^{-1}) were observed in the northwestern part of the area, which is in the rain-shadow of the hills. Some hilltops, for example in Yale and Ngangao, are without tree cover. In the foothills and

lowlands, AGB densities are low and less variable compared with the hills, particularly in the northeastern and southeastern parts of the area. In the lowlands, a larger AGB is concentrated in riverine areas, as they provide the consistent wetness necessary for trees. Predicting forest structure attributes using ALS-derived point cloud metrics is quite common in forest ecosystems. However, this study is not focused solely on forests, but it is conducted at the landscape level, i.e., across a mosaic of agriculture-forest land use. Figure 8 illustrates the AGB distribution in the Taita Hills at a 30-m spatial resolution (Study II). The pixels were summed for each class, and the total area and total AGB were calculated (Figure 8).

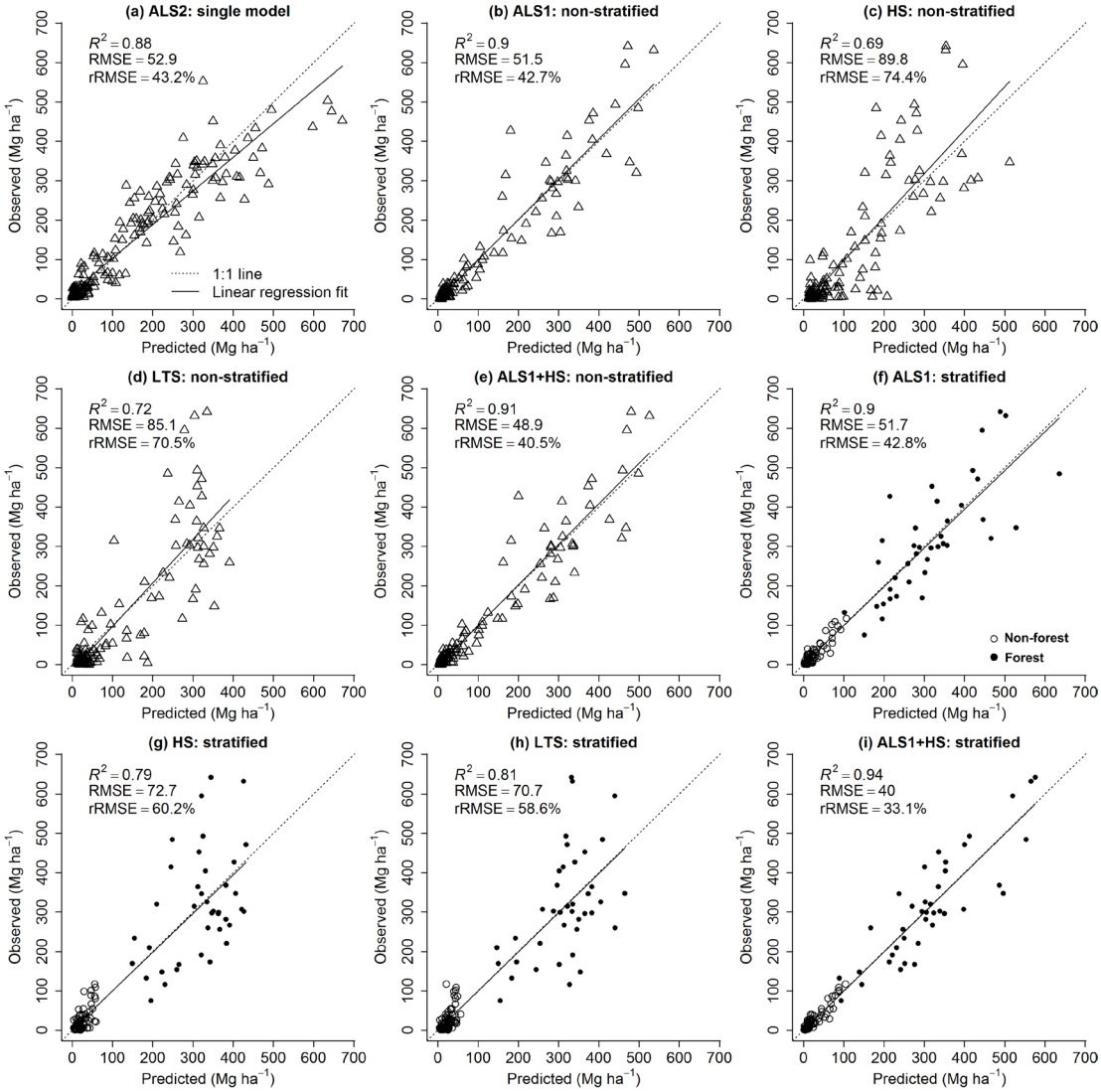

Figure 7. Observed versus predicted aboveground biomass (AGB) (Mg ha^{-1}) values based on individual and combined sensors. In Study II, (a) a single model was used for the whole landscape based on airborne laser scanning (ALS2) data. In Study III, individual and combined sensors were used (b–e) without and (f–i) with land cover stratification (forest/non-forest). The terms ALS, HS, and LTS represent airborne laser scanning data, hyperspectral data, and spectral-temporal metrics based on Landsat time series, respectively. See Table 2 for further details on ALS1 and ALS2.

Table 6. Summary of recent studies using airborne laser scanning (ALS) for aboveground biomass (AGB) modeling in Africa.

Reference	Country	Type of vegetation	Plot size (ha)	AGB (Mg ha^{-1})				R^2	RMSE (%)	Sensor
				Mean	SD	Range	RMSE[1]			
Asner et al., 2011[2]	Madagascar	Tropical moist forest	0.28	306.4	104.3	-	75.4	0.68	24.6	Carnegie Airborne Observatory (CAO)
Asner et al., 2012[3]	Madagascar	Wide range of vegetation types (dry and humid forest)	0.28	30.8, 211.7	17.2, 124.5	3.0–61.5, 19.8–547.6	44.9	0.88	-	CAO
Vaglio Laurin et al., 2014[4]	Sierra Leone	Moist evergreen forest, some areas of dry evergreen and semi-deciduous forest types	0.125	172.2	111.8	0–586.9	67.8	0.64	39.4	Optech Airborne Laser Terrain Mapper (ALTM) GEMINI
Hansen et al., 2015	Tanzania	Tropical submontane rainforest	0.06–0.12	461.9	214.7	43–1147	149.2	0.70	32.3	Leica ALS70
Mauya et al., 2015	Tanzania	Miombo woodlands with some forest, cultivated land, and other vegetation types	0.07	65.8	49.2	0.3–349.9		0.69	46.8	Leica ALS70
Næsset et al., 2016	Tanzania	Miombo woodlands	0.07	51.3	45.9	0–213.4	31.8	0.64	62.0	Leica ALS70
Ene et al., 2016	Tanzania	Miombo woodlands	-	-	0.3	0–349.87	31.16		47.4	Leica ALS70
Vaglio Laurin et al., 2016	Ghana	Moist evergreen and semi-deciduous forest	0.16	175.1	-	15–405	47.1	0.72	26.9	Optech ALTM GEMINI

1 Cross-validated value was selected when available

2 AGC was converted to AGB using carbon fraction of 0.47 (IPCC, 2006)

3 AGC was converted to AGB using carbon fraction of 0.47 (IPCC, 2006)

4 Integration of LiDAR metrics with hyperspectral bands improved model fit [R^2 = 0.70; RMSE = 61.7 (35.8 %)].

Tesfamichael and Beech 2016	Zambia	Savanna woodlands and grassland	0.08	0.85	1.18	0.45–6.1	0.53	0.81	62.4	ALTM
Adhikari et al., 2017	Kenya	Montane forests, exotic plantations, other semi-natural vegetation and agriculture	0.1	123.0	153.0	0.1–671.3	52.9	0.88	43.0	Leica ALS60
Egberth et al., 2017	Tanzania	Miombo woodlands	0.07	51.3	45.9	0–133.5	23.3	0.64	50.3	Leica ALS70
Pellikka et al., 2018	Kenya	Montane forests, exotic plantations, other semi-natural vegetation and agriculture	0.1	118.1	-	0.3–681.7	56.9	0.93	48.5	Optech ALTM 3100
Pellikka et al., 2018	Kenya	Lowland savanna and agricultural areas	0.1	9.3	-	0.0–51.4	4.26	0.89	44.7	Optech ALTM 3100
Fatoyinbo et al., 2018	Mozambique	Mangrove	0.52	203	166	-	122	0.85	33	
Heiskanen et al., 2019[5]	Kenya	Montane forests, exotic plantations, other semi-natural vegetation and agriculture	0.1	120.7	160.5	0.3–642.2	51.5	0.90	42.7	Optech ALTM 3100

5 Integration of LiDAR metrics with hyperspectral bands and metrics improved model fit [$R^2 = 0.94$; RMSE = 40 (33.1 %)].

Table 7. Summary of recent studies using multispectral satellite images for aboveground biomass (AGB) modeling in Africa.

Reference	Country	Type of vegetation	Plot size (ha)	AGB (Mg ha^{-1})				R^2	RMSE (%)	Sensor
				Mean	SD	Range	RMSE			
Avitabile et al., 2012	Uganda	National scale (cropland, grassland, woodland, forest)	0.04 / 0.25	-	-	0–383	13.9–16.9	0.83–0.86	-	Landsat-7 ETM+
Dube and Mutanga 2015b	South Africa	Plantation forest	0.04	-	-	-	9.55-20.15	0.53–0.76	18.07–14.40	Landsat-8 OLI/ Landsat-7 ETM+
Karlson et al., 2015	Burkina Faso	Open woodland, agro-forestry parklands, plantation and dense forest patches	0.25	26.6	27.2	0–153	17.6	0.57	66.0	Landsat-8 OLI
Gizachew et al., 2016	Tanzania	Miombo woodland	0.07	62.10	48.73	0–350.30	43.66			Landsat-8 OLI
Egberth et al., 2017	Tanzania	Miombo woodlands	0.07	51.3	45.9	0–133.5	30.6	0.38	66.2	Landsat-8 OLI
Heiskanen et al., 2017	Burkina Faso	Community-managed forest	0.1	18.7[1]	14.5	0–67.4	4.6	~ 0.55	51.7	Landsat-8 OLI
Chenge and Osho 2018	Nigeria	Mixed, moist, semi-evergreen rainforest with variable forest density	0.36	261.9	148.5	33.4–622.4	55.51	0.88	21.1	Landsat-8 OLI
Heiskanen et al., 2019	Kenya	Montane forests, exotic plantations, other semi-natural vegetation and agriculture	0.1	120.7	160.5	0.3–642.2	70.7	0.81	58.6	Landsat-8 OLI

1 AGC was converted to AGB using carbon fraction of 0.47 (IPCC, 2006)

4.3 Explanation of above ground biomass (AGB) distribution and forest tree size inequality based on maps

The determinants for the spatial distribution of AGB in the tropical landscape mosaic were studied based on climatic variables, topographical and hydrological variables, and land use class (Study II). The total explained deviance (cross-validated D2) of the BRT model was 72.7%. Mean annual precipitation (37.6%), cropland (16.9%), and slope (15.3%) were observed to be the most influential variables, while rivers, roads, and soil type explained only 5.9% of the total deviance. The AGB increased rapidly with increasing precipitation, and it was greatest in the mid-altitude hills where the MAP is high in comparison with the lowlands. The steep slope (up to 37 degrees) in the northeastern aspect and regions with a low cropland fraction contained a high AGB. This result is in line with Marshall et al., (2012), who observed that the AGB was greatest in gentle slopes and mid-elevation, which explained 63.7% of the variation on aboveground carbon (AGC) in the EAM, especially in Tanzania. However, a comparatively lower AGB was present in the steepest slopes. The AGB is more concentrated in northeastern and southeastern slopes, with a decreasing AGB on the leeward side. However, in another study in Africa (Madagascar), Asner et al., (2012) observed that elevation and the fraction of photosynthetic vegetation cover explained 27%–67% of the spatial variations. In Study II, temperature and elevation were removed, as they were highly correlated with MAP. The factor for the spatial distribution of live AGB can vary in different biomes as well as in a dense forest topography and human dominated landscape. In the study area, agroforestry, which could hold more biomass in the cropland, has been fairly common in recent decades.

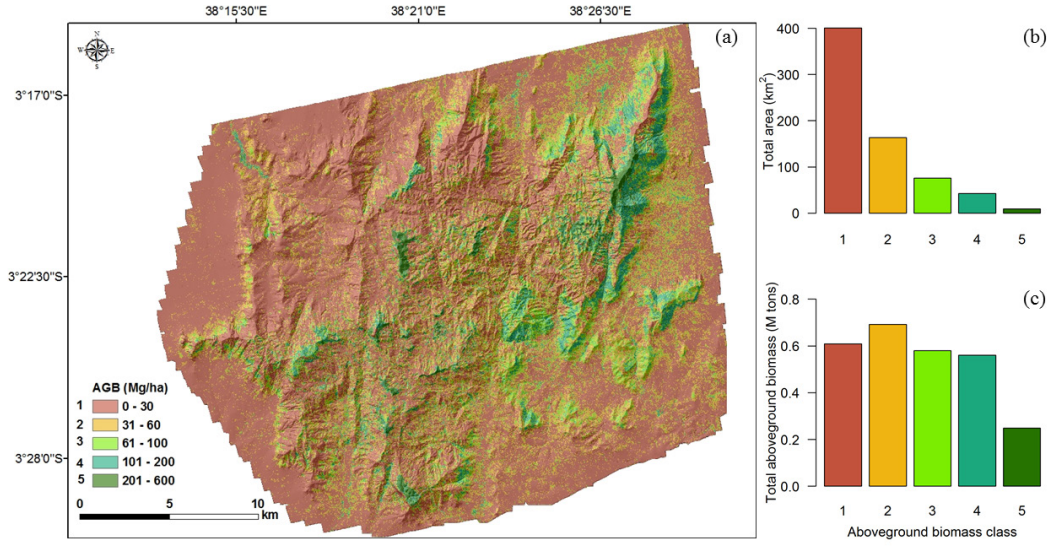

Figure 8. (a) Airborne laser scanning (ALS)-based aboveground biomass (AGB) distribution mapped at a 30-m × 30-m spatial resolution. Histograms were calculated by summing (b) the total area in kilometer square (km^2) and (c) the total AGB in million tons (M tons).

Forest structural heterogeneity can be mapped using 3D structural attributes from ALS and multispectral information from RS sensors. A GC based on a Lorenz curve quantifies tree size inequality among trees within a forest and can be used to differentiate the forest type and evaluate the effects of management practice on forest structure. In Study IV, ALS1 and ALS2 data, along with the spectral-temporal metrics based on LTS, were used for predicting forest structure heterogeneity in the form of the GC in three forest remnants (Ngangao, Yale, and Vuria). Comparatively lower prediction accuracies were achieved using ALS2 data ($rRMSE_{CV}$ 15.10%, R^2_{CV} 0.40); the reasons could be weak canopy penetration in a closed-canopy forest and a low pulse rate compared to ALS1 data ($rRMSE_{CV}$ 13.90%, R^2_{CV} 0.49). The accuracy obtained using the LTS in GC prediction was lower in the three forest remnants ($rRMSE_{CV}$ 16.30%, R^2_{CV} 0.30). Important synergies exist between ALS and LTS metrics for predicting the GC. The combination of ALS1 and LTS data improved the $rRMSE_{CV}$ from 13.90% to 12.5% in comparison with the use of ALS1 data only. However, with the combination of ALS2 and LTS, the $rRMSE_{CV}$ reduced from 15.10% to 13.00% in comparison with the use of ALS2 data only. These results demonstrate the potential of LTS metrics to increase the prediction accuracy of forest structural heterogeneity attributes. It is concluded that if the heterogeneity of tree sizes must be determined using ALS alone, then a high point density is needed. In other cases, low-density ALS data sets could be supported by satellite data providing information about the variation in forest density to obtain reliable results.

In the boreal forest, the potential of ALS data and vegetation indices derived from high-resolution multispectral data in predicting the GC has been demonstrated (Manzanera et al., 2016; Valbuena et al., 2016). However, the accuracy obtained by Valbuena et al., (2017) using ALS and airborne MS digital camera-based NDVI metrics was R^2_{CV} of 0.45, which was lower than the accuracy of 0.59 achieved in this study. This study is the first to exploit such potential with satellite

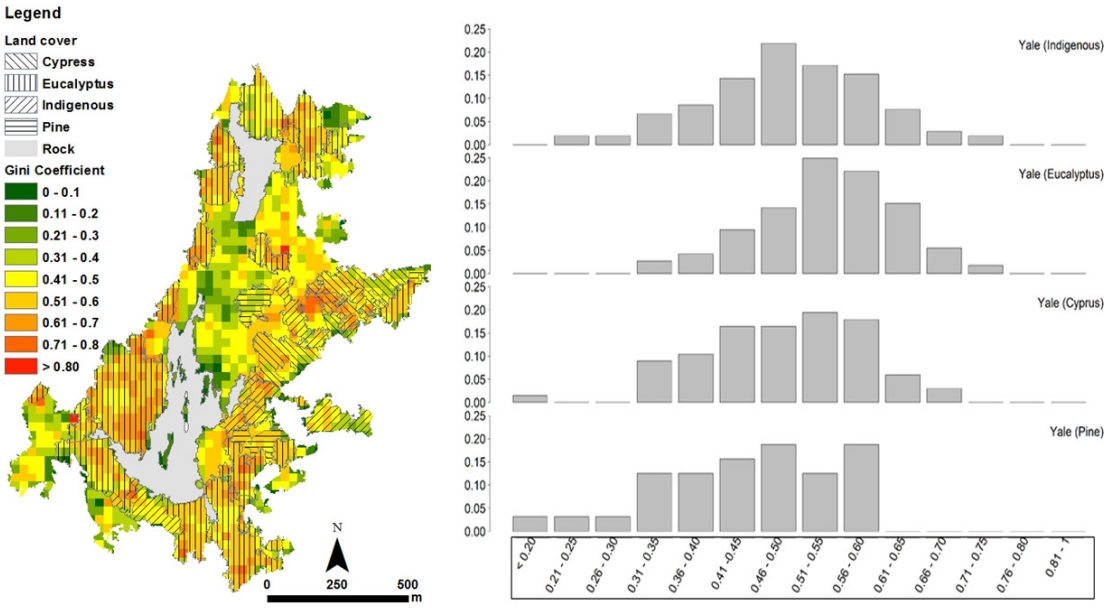

Figure 9. (Left) Gini coefficient (GC) map for Yale. (Right) The GC for indigenous and exotic plantations (eucalyptus, cypress, and pine) in the Yale forest in the Taita Hills based on pixel value.

imagery of a coarser resolution (Study IV). However, to the best of my knowledge, Study IV is the first study in Eastern Africa to estimate the GC in a tropical montane forest. The beta regression was able to model the GC with reasonable accuracy using ALS and LTS-based metrics, and it demonstrates how different pulse-density ALS data differ in terms of predictive modeling. Figure 9 depicts the GC map for the Yale forest and the histogram of the GC distribution in that forest in indigenous, eucalyptus, cypress, and pine forest stands.

Remote sensing approaches have proven useful for demonstrating the pattern of GC estimates outside of field inventory networks (Valbuena et al., 2016). The ALS and LTS metrics-based prediction of the GC reveals the spatially continuous, heterogeneous forest structure present in scattered, small-scale forests in the study area. Forest stands have an even-sized, irregular, or bimodal diameter distribution of tree sizes with each forest remnant. The results of this study suggest that plot-based estimates of the GC are often not enough to perform a landscape-level analysis. For example, at the level of plot data, an indigenous forest has a bimodal diameter distribution in all forest remnants. However, with the RS prediction, we were able to prove that the indigenous forests in Ngangao and in Vuria are bimodal and even-sized respectively (Figures 4 and 8, Study IV). We thus emphasize the potential of RS for increasing the statistical power in pursuing ecological hypotheses and displaying patterns on landscapes that cannot otherwise be detected.

4.4 Limitations and topics for further studies

In the tropics, large numbers of pixels in optical images were useless because of the persistence of clouds, cloud shadows, and haze, as well as sensor malfunction (Landsat-7 SLC-off). In addition, pixels falling on voids of the SRTM DEM were lost during topographic normalization. Further research should thus compare alternatives to the SRTM DEM that are void-free, for example a JAXA DEM or DSM/DTM based on ALS. Integrating direct and indirect measures of soil-based site productivity, along with ALS-, HS-, and MS-based structural and spectral information would have further improved the AGB and GC estimation. However, we observed that soil had low predictive power in the spatial distribution of AGB (Study II). The source of error in our study could have been introduced by the use of a pantropic allometric model and a manual error during the forest inventory conducted by different field teams. When possible, priorities should hence be given to species-specific and site-specific allometric models to improve prediction accuracy. However, uncertainties introduced because of the estimate of wood density, the DBH, and the height measurement should be considered. Further research should be conducted in different ecosystems and environmental settings to understand whether an accurate prediction can be made using ALS and LTS metrics.

High spatial-resolution satellite images, for example RapidEye (5 m), WorldView (1.84 m), Quickbird (2.4 m), PlanetScope image (3 m), and SkySat (0.8 m), provide opportunities to discriminate tree species, which might in turn increase GC prediction. Furthermore, the inclusion of textural information (spatial variations in tones), in addition to image spectral values, might improve the estimation of forest structure attributes.

5 Conclusions

This thesis addressed the potential and limitations of airborne and spaceborne RS data for predicting forest structural attributes. More specifically, the effect of topographic normalization on forest fractional cover prediction was addressed. Furthermore, it was demonstrated that fundamental forest structure attributes, such as the AGB and GC, can be estimated with acceptable accuracy through the integration of 3D structural information retrieved from ALS data and two-dimensional canopy spectral information from HS and MS RS data in the tropical mosaic landscape.

Airborne ALS and HS data are reliable RS techniques for the estimation of forest structural attributes in the agriculture-forest mosaic within a tropical landscape. However, for regular monitoring of a landscape area, wall-to-wall ALS and HS data are economically prohibitive. Persistent cloud cover severely limits the extent of optical RS data in the tropics. The spectral-temporal metrics based on LTS have the potential to improve the accuracy of forest structure prediction models through complementary data on the land surface phenology. Multi-temporal data help to distinguish between some vegetation types (for example evergreen, coniferous, or deciduous) by having continuous images throughout the growing seasons. This study presented the synergistic use of LTS and airborne ALS and HS data for the estimation of forest structural attributes in a tropical landscape.

In Study I, different vegetation and TC indices were affected differently because of the effect of the topography. The accuracy of the Fcover prediction model did not improve after topographic normalization in the case of ratio-based vegetation indices (NDVI and RSR) and TC greenness, but increased in the case of TC brightness and wetness. In contrast, the topographic normalization of single-date Landsat images and spectral-temporal metrics based on the LTS improved Fcover prediction, especially when brightness and wetness were used as predictor variables. However, the NDVI and RSR were found to be robust against topographic effects in tropical mountain landscapes throughout the year. Moreover, the SRTM DEM performed better in comparison with the ASTER and regional DEMs based on topographic maps. The highest accuracy was achieved using the RSR, and if the TC indices are preferred, then we recommend topographic normalization using the SRTM DEM.

In Study II, a linear relationship was observed between plot-level AGB estimates derived from inventory plots in the tropical landscape and ALS metrics extracted from corresponding locations. High-resolution, accurate, and spatially explicit AGB estimates at the landscape level were obtained based on spatially explicit ALS2 data using a multiple linear regression model. It was concluded that ALS2 alone contributes more to the prediction of AGB in the agriculture-forest mosaic landscape. Furthermore, landscape-scale spatial variations and determinants of AGB distribution were explored. It was observed that AGB distribution patterns were controlled mainly by MAP, the distribution of croplands, and slope, which collectively explained 69.8% of the AGB variation. In addition, plantation forests, topographic position, and the density of buildings had a minor influence on AGB.

In Study III, the AGB of trees outside and in closed native forests was modeled at the landscape level. The ALS1 data alone provided robust models for AGB mapping across the tropical mosaic landscape, even without stratification (separate models for non-forest and forest areas). The incorporation of ALS1 data with HS data extended the properties of forest structure attributes from 3D to detailed canopy spectral information, while the stratification of land cover captured the variation in relations between different sensors and the

field-estimated AGB. The combination of ALS1, HS, and the stratification performed well. However, it was observed that in the ALS1+LTS models, the LTS metrics contributed only slightly to explaining the variation beyond that explained by ALS1 alone. Furthermore, comparing Studies II and III, which used ALS2 (low) and ALS1 (high pulse density) respectively, the estimated accuracy of biophysical parameters such as biomass did not increase significantly with high pulse-density ALS data.

Study IV showed the independent and combined use of ALS and LTS data in prediction models for accurately estimating the GC. Airborne laser scanning provides detailed and extensive information on forest structure characteristics. The high pulse-density ALS1 had relatively higher accuracy compared with ALS2, and the LTS had limited predictive power when used alone. Study IV also demonstrated that maximum accuracy and minimum error were obtained with ALS1-derived metrics in combination with LTS-metrics for estimating the GC.

This thesis highlights the potential of ALS, HS, and LTS for RS tropical forest structure attributes in the montane forest-agricultural mosaic landscape. The cost per unit area of ALS and HS data is high at present; however, this will not be the case in the future, as a rapid decrease in acquisition costs has been observed in the last two decades. Furthermore, ALS and HS equipment mounted on unmanned aerial vehicles is currently gaining attention and is expected to reduce the acquisition cost further. This thesis also demonstrates that high-level accuracy can be obtained using ALS and high-resolution HS RS data. It further compared the impacts of different pulse densities in ALS data for modeling and mapping forest structure attributes. In general, these technologies result in the accurate monitoring and verifying of forest structure parameters, which are important for implementing climate-change mitigation strategies in Africa. Further research should utilize free and affordable satellite data, which would result in sustainable development in Africa.

References

Adhikari, H., Heiskanen, J., Siljander, M., Maeda, E., Heikinheimo, V., & K. E. Pellikka, P. (2017). Determinants of Aboveground Biomass across an Afromontane Landscape Mosaic in Kenya. Remote Sensing, 9(8), 827.

Aerts, R., Thijs, K.W., Lehouck, V., Beentje, H., Bytebier, B., Matthysen, E., Gulinck, H., Lens, L., & Muys, B. (2011). Woody plant communities of isolated Afromontane cloud forests in Taita Hills, Kenya. Plant Ecology, 212(4), 639-649.

Asner, G.P., Clark, J.K., Mascaro, J., Vaudry, R., Chadwick, K.D., Vieilledent, G., Rasamoelina, M., Balaji, A., Kennedy-Bowdoin, T., Maatoug, L., Colgan, M.S., & Knapp, D.E. (2012). Human and environmental controls over aboveground carbon storage in Madagascar. Carbon Balance Manag, 7(1), 2.

Asner, G.P., Hughes, R.F., Varga, T.A., Knapp, D.E., & Kennedy-Bowdoin, T. (2009). Environmental and Biotic Controls over Aboveground Biomass Throughout a Tropical Rain Forest. Ecosystems, 12(2), 261-278.

Asner, G.P., Mascaro, J., Muller-Landau, H.C., Vieilledent, G., Vaudry, R., Rasamoelina, M., Hall, J.S., & van Breugel, M. (2011). A universal airborne LiDAR approach for tropical forest carbon mapping. Oecologia, 168(4), 1147-1160.

Avitabile, V., Baccini, A., Friedl, M.A., & Schmullius, C. (2012). Capabilities and limitations of Landsat and land cover data for aboveground woody biomass estimation of Uganda. Remote Sensing of Environment, 117, 366-380.

Avitabile, V., Herold, M., Heuvelink, G.B.M., Lewis, S.L., Phillips, O.L., Asner, G.P., Armston, J., Ashton, P.S., Banin, L., Bayol, N., Berry, N.J., Boeckx, P., de Jong, B.H.J., DeVries, B., Girardin, C.A.J., Kearsley, E., Lindsell, J.A., Lopez-Gonzalez, G., Lucas, R., Malhi, Y., Morel, A., Mitchard, E.T.A., Nagy, L., Qie, L., Quinones, M.J., Ryan, C.M., Ferry, S.J.W., Sunderland, T., Laurin, G.V., Gatti, R.C., Valentini, R., Verbeeck, H., Wijaya, A., & Willcock, S. (2016). An integrated pan-tropical biomass map using multiple reference datasets, 22(4), 1406-1420.

Baccini, A., Goetz, S.J., Walker, W.S., Laporte, N.T., Sun, M., Sulla-Menashe, D., Hackler, J., Beck, P.S.A., Dubayah, R., Friedl, M.A., Samanta, S., & Houghton, R.A. (2012). Estimated carbon dioxide emissions from tropical deforestation improved by carbon-density maps. Nature Climate Change, 2, 182.

Baccini, A., Walker, W., Carvalho, L., Farina, M., Sulla-Menashe, D., & Houghton, R.A. (2017). Tropical forests are a net carbon source based on aboveground measurements of gain and loss, 358(6360), 230-234.

Banskota, A., Kayastha, N., Falkowski, M.J., Wulder, M.A., Froese, R.E., & White, J.C. (2014). Forest Monitoring Using Landsat Time Series Data: A Review. Canadian Journal of Remote Sensing, 40(5), 362-384.

Bouvet, A., Mermoz, S., Le Toan, T., Villard, L., Mathieu, R., Naidoo, L., & Asner, G.P. (2018). An above-ground biomass map of African savannahs and woodlands at 25m resolution derived from ALOS PALSAR. Remote Sensing of Environment, 206, 156-173.

Brink, A.B., Bodart, C., Brodsky, L., Defourney, P., Ernst, C., Donney, F., Lupi, A., & Tuckova, K. (2014). Anthropogenic pressure in East Africa—Monitoring 20 years of land cover changes by means of medium resolution satellite data. International Journal of Applied Earth Observation and Geoinformation, 28, 60-69.

Brown, L., Chen, J.M., Leblanc, S.G., & Cihlar, J. (2000). A Shortwave Infrared Modification to the Simple Ratio for LAI Retrieval in Boreal Forests: An Image and Model Analysis. Remote Sensing of Environment, 71(1), 16-25.

Brown, S. (1997). Estimating biomass and biomass change of tropical forests: a primer. FAO Forestry Paper, 134.

Chance, C.M., Hermosilla, T., Coops, N.C., Wulder, M.A., & White, J.C. (2016). Effect of topographic correction on forest change detection using spectral trend analysis of Landsat pixel-based composites. International Journal of Applied Earth Observation and Geoinformation, 44, 186-194.

Chave, J., Réjou-Méchain, M., Búrquez, A., Chidumayo, E., Colgan, M.S., Delitti, W.B.C., Duque, A., Eid, T., Fearnside, P.M., Goodman, R.C., Henry, M., Martínez-Yrízar, A., Mugasha, W.A., Muller-Landau, H.C., Mencuccini, M., Nelson, B.W., Ngomanda, A., Nogueira, E.M., Ortiz-Malavassi, E., Pélissier, R., Ploton, P., Ryan, C.M., Saldarriaga, J.G., & Vieilledent, G. (2014). Improved allometric models to estimate the aboveground biomass of tropical trees. Global Change Biology, 20(10), 3177-3190.

Chen, Q., Vaglio Laurin, G., & Valentini, R. (2015). Uncertainty of remotely sensed aboveground biomass over an African tropical forest: Propagating errors from trees to plots to pixels. Remote Sensing of Environment, 160, 134-143.

Chenge, I.B., & Osho, J.S.A. (2018). Mapping tree aboveground biomass and carbon in Omo Forest Reserve Nigeria using Landsat 8 OLI data. Southern Forests: a Journal of Forest Science, 80(4), 341-350.

Clark, B.J.F., & Pellikka, P.K.E. (2009). Landscape analysis using multiscale segmentation and object orientated classification. Recent Advances in Remote Sensing and Geoinformation Processing for Land Degradation Assessment, 8, 323-342.

Clark, M.L., Roberts, D.A., Ewel, J.J., & Clark, D.B. (2011). Estimation of tropical rain forest aboveground biomass with small-footprint lidar and hyperspectral sensors. Remote Sensing of Environment, 115(11), 2931-2942.

Crist, E.P. (1985). A TM Tasseled Cap equivalent transformation for reflectance factor data. Remote Sensing of Environment, 17(3), 301-306.

Cuni-Sanchez, A., Pfeifer, M., Marchant, R., Calders, K., Sørensen, C.L., Pompeu, P.V., Lewis, S.L., & Burgess, N.D. (2017). New insights on above ground biomass and forest attributes in tropical montane forests. Forest Ecology and Management, 399, 235-246.

Dube, T., & Mutanga, O. (2015a). Evaluating the utility of the medium-spatial resolution Landsat 8 multispectral sensor in quantifying aboveground biomass in uMgeni catchment, South Africa. ISPRS Journal of Photogrammetry and Remote Sensing, 101, 36-46.

Dube, T., & Mutanga, O. (2015b). Investigating the robustness of the new Landsat-8 Operational Land Imager derived texture metrics in estimating plantation forest aboveground biomass in resource constrained areas. ISPRS Journal of Photogrammetry and Remote Sensing, 108, 12-32.

Egberth, M., Nyberg, G., Næsset, E., Gobakken, T., Mauya, E., Malimbwi, R., Katani, J., Chamuya, N., Bulenga, G., Olsson, H.J.C.B., & Management (2017). Combining airborne laser scanning and Landsat data for statistical modeling of soil carbon and tree biomass in Tanzanian Miombo woodlands, 12(1), 8.

Elkhrachy, I. (2018). Vertical accuracy assessment for SRTM and ASTER Digital Elevation Models: A case study of Najran city, Saudi Arabia. Ain Shams Engineering Journal, 9(4), 1807-1817.

Ene, L.T., Næsset, E., Gobakken, T., Mauya, E.W., Bollandsås, O.M., Gregoire, T.G., Ståhl, G., & Zahabu, E. (2016). Large-scale estimation of aboveground biomass in miombo woodlands using airborne laser scanning and national forest inventory data. Remote Sensing of Environment, 186, 626-636.

Enroth, J., Nyqvist, P., Malombe, I., Pellikka, P., & Rikkinen, J. (2013). Additions to the moss flora of the Taita Hills and Mount Kasigau, Kenya. In, Polish Botanical Journal (p. 495)

Fatoyinbo, T., Feliciano, E.A., Lagomasino, D., Lee, S.K., & Trettin, C. (2018). Estimating mangrove aboveground biomass from airborne LiDAR data: a case study from the Zambezi River delta. Environmental Research Letters, 13(2), 025012.

Frey, H., & Paul, F. (2012). On the suitability of the SRTM DEM and ASTER GDEM for the compilation of topographic parameters in glacier inventories. International Journal of Applied Earth Observation and Geoinformation, 18(0), 480-490.

Fuller, D.O. (2006). Tropical forest monitoring and remote sensing: A new era of transparency in forest governance?, 27(1), 15-29.

Galvão, L.S., Breunig, F.M., Teles, T.S., Gaida, W., & Balbinot, R. (2016). Investigation of terrain illumination effects on vegetation indices and VI-derived phenological metrics in subtropical deciduous forests. GIScience & Remote Sensing, 53(3), 360-381.

Gizachew, B., Solberg, S., Næsset, E., Gobakken, T., Bollandsås, O.M., Breidenbach, J., Zahabu, E., Mauya, E.W.J.C.B., & Management (2016). Mapping and estimating the total living biomass and carbon in low-biomass woodlands using Landsat 8 CDR data, 11(1), 13.

Gourlet-Fleury, S., Rossi, V., Rejou-Mechain, M., Freycon, V., Fayolle, A., Saint-André, L., Cornu, G., Gérard, J., Sarrailh, J.-M., Flores, O., Baya, F., Billand, A., Fauvet, N., Gally, M., Henry, M., Hubert, D., Pasquier, A., & Picard, N. (2011). Environmental filtering of dense-wooded species controls above-ground biomass stored in African moist forests, 99(4), 981-990.

Gu, D., & Gillespie, A. (1998). Topographic Normalization of Landsat TM Images of Forest Based on Subpixel Sun–Canopy–Sensor Geometry. Remote Sensing of Environment, 64(2), 166-175.

Hansen, E.H., Gobakken, T., Bollandsas, O.M., Zahabu, E., & Naesset, E. (2015). Modeling Aboveground Biomass in Dense Tropical Submontane Rainforest Using Airborne Laser Scanner Data. Remote Sensing, 7(1), 788-807.

Hansen, M.C., Potapov, P.V., Goetz, S.J., Turubanova, S., Tyukavina, A., Krylov, A., Kommareddy, A., & Egorov, A. (2016). Mapping tree height distributions in Sub-Saharan Africa using Landsat 7 and 8 data. Remote Sensing of Environment, 185, 221-232.

Hansen, M.C., Potapov, P.V., Moore, R., Hancher, M., Turubanova, S.A., Tyukavina, A., Thau, D., Stehman, S.V., Goetz, S.J., Loveland, T.R., Kommareddy, A., Egorov, A., Chini, L., Justice, C.O., & Townshend, J.R.G. (2013). High-Resolution Global Maps of 21st-Century Forest Cover Change, 342(6160), 850-853.

Heiskanen, J., Adhikari, H., Piiroinen, R., Packalen, P., & Pellikka, P.K.E. (2019). Do airborne laser scanning biomass prediction models benefit from Landsat time series, hyperspectral data or forest classification in tropical mosaic landscapes? International Journal of Applied Earth Observation and Geoinformation, 81, 176-185.

Heiskanen, J., Korhonen, L., Hietanen, J., & Pellikka, P.K.E. (2015). Use of airborne lidar for estimating canopy gap fraction and leaf area index of tropical montane forests. International Journal of Remote Sensing, 36(10), 2569-2583.

Heiskanen, J., Liu, J., Valbuena, R., Aynekulu, E., Packalen, P., & Pellikka, P. (2017). Remote sensing approach for spatial planning of land management interventions in West African savannas. Journal of Arid Environments, 140, 29-41.

Heiskanen, J., Pellikka, P.K.E., Aynekulu, E., & Packalen, P. (2013). Field measurement guidelines for aboveground biomass and fuel wood stocks. Building Biocarbon and Rural Development in West Africa (BIODEV)

Henry, M., Picard, N., Trotta, C., Manlay, R., Valentini, R., Bernoux, M., & Saint-André, L. (2011). Estimating tree biomass of sub-Saharan African forests: a review of available allometric equations.

Higginbottom, T.P., Symeonakis, E., Meyer, H., & van der Linden, S. (2018). Mapping fractional woody cover in semi-arid savannahs using multi-seasonal composites from Landsat data. ISPRS Journal of Photogrammetry and Remote Sensing, 139, 88-102.

Hirt, C., Filmer, M.S., & Featherstone, W.E. (2010). Comparison and validation of the recent freely available ASTER-GDEM ver1, SRTM ver4.1 and GEODATA DEM-9S ver3 digital elevation models over Australia. Australian Journal of Earth Sciences, 57(3), 337-347.

Holl, K.D., & Zahawi, R.A. (2014). Factors explaining variability in woody above-ground biomass accumulation in restored tropical forest. Forest Ecology and Management, 319, 36-43.

Hopkinson, C., & Chasmer, L. (2009). Testing LiDAR models of fractional cover across multiple forest ecozones. Remote Sensing of Environment, 113(1), 275-288.

Houghton, R.A. (2005). Aboveground Forest Biomass and the Global Carbon Balance, 11(6), 945-958.

Hudak, A.T., Lefsky, M.A., Cohen, W.B., & Berterretche, M. (2002). Integration of lidar and Landsat ETM+ data for estimating and mapping forest canopy height. Remote Sensing of Environment, 82(2–3), 397-416.

IPCC (2000). Land use, land-use change, and forestry. Robert T. Watson, Ian R. Noble, Bert Bolin, N. H. Ravindranath, David J. Verardo and David J. Dokken (Eds.) Cambridge University Press, UK. pp 375 Available from Cambridge University Press, The Edinburgh Building Shaftesbury Road, Cambridge CB2 2RU ENGLAND.

Isenburg, M. (2014). "LAStools - efficient LiDAR processing software" (version 141017, unlicensed), obtained from http://rapidlasso.com/LAStools

JAXA (2015). http://global.jaxa.jp/press/2015/05/20150518_daichi.html (assessed 02.02018.).

Jspacesystem (2011). https://www.jspacesystems.or.jp/ersdac/GDEM/E/4.html (assessed 02.02016.)

Karlson, M., Ostwald, M., Reese, H., Sanou, J., Tankoano, B., & Mattsson, E. (2015). Mapping Tree Canopy Cover and Aboveground Biomass in Sudano-Sahelian Woodlands Using Landsat 8 and Random Forest, 7(8), 10017-10041.

Korhonen, L., Heiskanen, J., & Korpela, I. (2013). Modelling lidar-derived boreal forest canopy cover with SPOT 4 HRVIR data. International Journal of Remote Sensing, 34(22), 8172-8181.

Lewis, S.L., Sonké, B., Sunderland, T., Begne, S.K., Lopez-Gonzalez, G., van der Heijden, G.M.F., Phillips, O.L., Affum-Baffoe, K., Baker, T.R., Banin, L., Bastin, J.-F., Beeckman, H., Boeckx, P., Bogaert, J., De Cannière, C., Chezeaux, E., Clark, C.J., Collins, M., Djagbletey, G., Djuikouo, M.N.K., Droissart, V., Doucet, J.-L., Ewango, C.E.N., Fauset, S., Feldpausch, T.R., Foli, E.G., Gillet, J.-F., Hamilton, A.C., Harris, D.J., Hart, T.B., de Haulleville, T., Hladik, A., Hufkens, K., Huygens, D., Jeanmart, P., Jeffery, K.J., Kearsley, E., Leal, M.E., Lloyd, J., Lovett, J.C., Makana, J.-R., Malhi, Y., Marshall, A.R., Ojo, L., Peh, K.S.-H., Pickavance, G., Poulsen, J.R., Reitsma, J.M., Sheil, D., Simo, M., Steppe, K., Taedoumg, H.E., Talbot, J., Taplin, J.R.D., Taylor, D., Thomas, S.C., Toirambe, B., Verbeeck, H., Vleminckx, J., White, L.J.T., Willcock, S., Woell, H., & Zemagho, L. (2013). Above-ground biomass and structure of 260 African tropical forests. Philosophical Transactions

of the Royal Society B: Biological Sciences, 368(1625)

Loubota Panzou, G.J., Fayolle, A., Feldpausch, T.R., Ligot, G., Doucet, J.-L., Forni, E., Zombo, I., Mazengue, M., Loumeto, J.-J., & Gourlet-Fleury, S. (2018). What controls local-scale aboveground biomass variation in central Africa? Testing structural, composition and architectural attributes. Forest Ecology and Management, 429, 570-578.

Lovett, J.C., & Wasser, S.K. (1993). Biogeography and Ecology of the Rainforests of Eastern Africa. Cambridge University Press, Cambridge.

Lutz, D.A., Washington-Allen, R.A., & Shugart, H.H. (2008). Remote sensing of boreal forest biophysical and inventory parameters: a review. Canadian Journal of Remote Sensing, 34(sup2), S286-S313.

Manzanera, J.A., García-Abril, A., Pascual, C., Tejera, R., Martín-Fernández, S., Tokola, T., & Valbuena, R. (2016). Fusion of airborne LiDAR and multispectral sensors reveals synergic capabilities in forest structure characterization. GIScience & Remote Sensing, 53(6), 723-738.

Marshall, A.R., Willcock, S., Platts, P.J., Lovett, J.C., Balmford, A., Burgess, N.D., Latham, J.E., Munishi, P.K.T., Salter, R., Shirima, D.D., & Lewis, S.L. (2012). Measuring and modelling above-ground carbon and tree allometry along a tropical elevation gradient. Biological Conservation, 154, 20-33.

Masek, J.G., Vermote, E.F., Saleous, N.E., Wolfe, R., Hall, F.G., Huemmrich, K.F., Gao, F., Kutler, J., & Lim, T.-K. (2006). A Landsat Surface Reflectance Dataset for North America, 1990–2000, 3(1), 68-72.

Mauya, E.W., Ene, L.T., Bollandsås, O.M., Gobakken, T., Næsset, E., Malimbwi, R.E., & Zahabu, E. (2015). Modelling aboveground forest biomass using airborne laser scanner data in the miombo woodlands of Tanzania. Carbon Balance and Management, 10(1), 28.

McGaughey, R.J. (2016). FUSION/LDV: Software for LIDAR data analysis and visualization. US Department of Agriculture, Forest Service, Pacific Northwest Research Station: Seattle, WA, USA(Version 3.60)

Mehtätalo, L., de-Miguel, S., & Gregoire, T.G. (2015). Modeling height-diameter curves for prediction. Canadian Journal of Forest Research, 45(7), 826-837.

Minnaert, M.G.J. (1941). The reciprocity principle in lunar photometry. Astrophysical Journal, 93, 403 - 410.

Morsdorf, F., Kotz, B., Meier, E., Itten, K.I., & Allgower, B. (2006). Estimation of LAI and fractional cover from small footprint airborne laser scanning data based on gap fraction. Remote Sensing of Environment, 104(1), 50-61.

Næsset, E. (2002). Predicting forest stand characteristics with airborne scanning laser using a practical two-stage procedure and field data. Remote Sensing of Environment, 80(1), 88-99.

Næsset, E., & Gobakken, T. (2008). Estimation of above- and below-ground biomass across regions of the boreal forest zone using airborne laser. Remote Sensing of Environment, 112(6), 3079-3090.

Næsset, E., Ørka, H.O., Solberg, S., Bollandsås, O.M., Hansen, E.H., Mauya, E., Zahabu, E., Malimbwi, R., Chamuya, N., Olsson, H., & Gobakken, T. (2016). Mapping and estimating forest area and aboveground biomass in miombo woodlands in Tanzania using data from airborne laser scanning, TanDEM-X, RapidEye, and global forest maps: A comparison of estimated precision. Remote Sensing of Environment, 175, 282-300.

Nölte, A., Meilby, H., & Yousefpour, R. (2018). Multi-purpose forest management in the tropics: Incorporating values of carbon, biodiversity and timber in managing Tectona grandis (teak) plantations in Costa Rica. Forest Ecology and Management, 422, 345-357.

Pan, Y., Birdsey, R.A., Fang, J., Houghton, R., Kauppi, P.E., Kurz, W.A., Phillips, O.L., Shvidenko, A., Lewis, S.L., Canadell, J.G., Ciais, P., Jackson, R.B., Pacala, S.W., McGuire, A.D., Piao, S., Rautiainen, A., Sitch, S., & Hayes, D. (2011). A Large and Persistent Carbon Sink in the World's Forests, 333(6045), 988-993.

Paul, K.I., Roxburgh, S.H., England, J.R., Ritson, P., Hobbs, T., Brooksbank, K., John Raison, R., Larmour, J.S., Murphy, S., Norris, J., Neumann, C., Lewis, T., Jonson, J., Carter, J.L., McArthur, G., Barton, C., & Rose, B. (2013). Development and testing of allometric equations for estimating above-ground biomass of mixed-species environmental plantings. Forest Ecology and Management, 310, 483-494.

Pellikka, P.K.E., Clark, B.J.F., Gosa, A.G., Himberg, N., Hurskainen, P., Maeda, E., Mwang'ombe, J., Omoro, L.M.A., & Siljander, M. (2013). Chapter 13 - Agricultural Expansion and Its Consequences in the Taita Hills, Kenya. In D.O.O. Paolo Paron, & O. Christian Thine (Eds.), Developments in Earth Surface Processes (pp. 165-179): Elsevier.

Pellikka, P.K.E., Heikinheimo, V., Hietanen, J., Schäfer, E., Siljander, M., & Heiskanen, J. (2018). Impact of land cover change on aboveground carbon stocks in Afromontane landscape in Kenya. Applied Geography, 94, 178-189.

Pellikka, P.K.E., Lötjönen, M., Siljander, M., & Lens, L. (2009). Airborne remote sensing of spatiotemporal change (1955–2004) in indigenous and exotic forest cover in the Taita Hills, Kenya. International Journal of Applied Earth Observation and Geoinformation, 11(4), 221-232.

Pfeifer, M., Platts, P.J., Burgess, N.D., Swetnam, R.D., Willcock, S., Lewis, S.L., & Marchant, R. (2012). Land use change and carbon fluxes in East Africa quantified using earth observation data and field measurements. Environmental Conservation, 40(3), 241-252.

Phua, M.-H., Johari, S.A., Wong, O.C., Ioki, K., Mahali, M., Nilus, R., Coomes, D.A., Maycock, C.R., & Hashim, M. (2017). Synergistic use of Landsat 8 OLI image and airborne LiDAR data for above-ground biomass estimation in tropical lowland rainforests. Forest Ecology and Management, 406, 163-171.

Piiroinen, P. (2018). Airborne imaging spectroscopy in mapping of heterogenous tropical land cover in Eastern Africa. In, Department of Geosciences and Geography A69. Unigrafia. Helsinki

Piiroinen, R., Fassnacht, F.E., Heiskanen, J., Maeda, E., Mack, B., & Pellikka, P. (2018). Invasive tree species detection in the Eastern Arc Mountains biodiversity hotspot using one class classification. Remote Sensing of Environment, 218, 119-131.

Piiroinen, R., Heiskanen, J., Mõttus, M., & Pellikka, P. (2015). Classification of crops across heterogeneous agricultural landscape in Kenya using AisaEAGLE imaging spectroscopy data. International Journal of Applied Earth Observation and Geoinformation, 39, 1-8.

Pinheiro, J., Bates, D., DebRoy, S., & Sarkar, D. (2014). R Core Team nlme: Linear and nonlinear mixed effects models. R package version 3.1-118

Potapov, P., Turubanova, S., & Hansen, M.C. (2011). Regional-scale boreal forest cover and change mapping using Landsat data composites for European Russia. Remote Sensing of Environment, 115(2), 548-561.

Potapov, P.V., Turubanova, S.A., Hansen, M.C., Adusei, B., Broich, M., Altstatt, A., Mane, L., & Justice, C.O. (2012). Quantifying forest cover loss in Democratic Republic of the Congo, 2000–2010, with Landsat ETM+ data. Remote Sensing of Environment, 122, 106-116.

Reese, H., & Olsson, H. (2011). C-correction of optical satellite data over alpine vegetation areas: A comparison of sampling strategies for determining the

empirical c-parameter. Remote Sensing of Environment, 115(6), 1387-1400.

Rouse, J.W., Haas, R.H., Schell, J.A., & Deering, D.W. (1973). Monitoring vegetation systems in the Great Plains with ERTS. In: Fraden S.C., Marcanti E.P. and Becker M.A. (eds.), Third ERTS-1 Symposium, 10-14 Dec. 1973, NASA SP-351, Washington D.C. NASA, pp.309-317.

Saatchi, S.S., Harris, N.L., Brown, S., Lefsky, M., Mitchard, E.T.A., Salas, W., Zutta, B.R., Buermann, W., Lewis, S.L., Hagen, S., Petrova, S., White, L., Silman, M., & Morel, A. (2011). Benchmark map of forest carbon stocks in tropical regions across three continents, 108(24), 9899-9904.

Shang, C., Treitz, P., Caspersen, J., & Jones, T. (2019). Estimation of forest structural and compositional variables using ALS data and multi-seasonal satellite imagery. International Journal of Applied Earth Observation and Geoinformation, 78, 360-371.

Sloan, S., & Sayer, J.A. (2015). Forest Resources Assessment of 2015 shows positive global trends but forest loss and degradation persist in poor tropical countries. Forest Ecology and Management, 352, 134-145.

Song, C., & Woodcock, C.E. (2003). Monitoring forest succession with multitemporal Landsat images: factors of uncertainty. IEEE Transactions on Geoscience and Remote Sensing, 41(11), 2557-2567.

SRTM (2014). https://lta.cr.usgs.gov/SRTM1Arc (assessed 30.11.15.).

Stam, Å., Enroth, J., Malombe, I., Pellikka, P., & Rikkinen, J. (2017). Experimental transplants reveal strong environmental effects on the growth of non□vascular epiphytes in Afromontane forests. Biotropica, 49(6), 862-870.

Teillet, P.M., Guindon, B., & Goodenough, D.G. (1982). On the Slope-Aspect Correction of Multispectral Scanner Data. Canadian Journal of Remote Sensing, 8(2), 84-106.

Tesfamichael, S.G., & Beech, C. (2016). Combining Akaike's Information Criterion and discrete return LiDAR data to estimate structural attributes of savanna woody vegetation. Journal of Arid Environments, 129, 25-34.

Thijs, K.W., Aerts, R., Musila, W., Siljander, M., Matthysen, E., Lens, L., Pellikka, P., Gulinck, H., & Muys, B. (2014). Potential tree species extinction, colonization and recruitment in Afromontane forest relicts. Basic and Applied Ecology, 15(4), 288-296.

Thijs, K.W., Aerts, R., van de Moortele, P., Aben, J., Musila, W., Pellikka, P., Gulinck, H., & Muys, B. (2015). Trees in a human-modified tropical landscape: Species and trait composition and potential ecosystem services. Landscape and Urban Planning, 144, 49-58.

Vaglio Laurin, G., Chen, Q., Lindsell, J.A., Coomes, D.A., Frate, F.D., Guerriero, L., Pirotti, F., & Valentini, R. (2014). Above ground biomass estimation in an African tropical forest with lidar and hyperspectral data. ISPRS Journal of Photogrammetry and Remote Sensing, 89, 49-58.

Vaglio Laurin, G., Puletti, N., Chen, Q., Corona, P., Papale, D., & Valentini, R. (2016). Above ground biomass and tree species richness estimation with airborne lidar in tropical Ghana forests. International Journal of Applied Earth Observation and Geoinformation, 52, 371-379.

Valbuena, R., Eerikäinen, K., Packalen, P., & Maltamo, M. (2016). Gini coefficient predictions from airborne lidar remote sensing display the effect of management intensity on forest structure. Ecological Indicators, 60(Supplement C), 574-585.

Valbuena, R., Hernando, A., Manzanera, J.A., Martínez-Falero, E., García-Abril, A., & Mola-Yudego, B. (2017). Most similar neighbor imputation of forest attributes using metrics derived from combined airborne LIDAR and multispectral sensors.

International Journal of Digital Earth, 1-14.

Valbuena, R., Packalén, P., Martı´n-Fernández, S., & Maltamo, M. (2012). Diversity and equitability ordering profiles applied to study forest structure. Forest Ecology and Management, 276, 185-195.

Valbuena, R., Packalen, P., Mehtätalo, L., García-Abril, A., & Maltamo, M. (2013). Characterizing forest structural types and shelterwood dynamics from Lorenz-based indicators predicted by airborne laser scanning. Canadian Journal of Forest Research, 43(11), 1063-1074.

Vanderhaegen, K., Verbist, B., Hundera, K., & Muys, B. (2015). REALU vs. REDD+: Carbon and biodiversity in the Afromontane landscapes of SW Ethiopia. Forest Ecology and Management, 343, 22-33.

Vanonckelen, S., Lhermitte, S., & Van Rompaey, A. (2013). The effect of atmospheric and topographic correction methods on land cover classification accuracy. International Journal of Applied Earth Observation and Geoinformation, 24(0), 9-21.

Vanonckelen, S., Lhermitte, S., & Van Rompaey, A. (2015). The effect of atmospheric and topographic correction on pixel-based image composites: Improved forest cover detection in mountain environments. International Journal of Applied Earth Observation and Geoinformation, 35, Part B(0), 320-328.

White, J.C., Wulder, M.A., Hobart, G.W., Luther, J.E., Hermosilla, T., Griffiths, P., Coops, N.C., Hall, R.J., Hostert, P., Dyk, A., & Guindon, L. (2014). Pixel-Based Image Compositing for Large-Area Dense Time Series Applications and Science. Canadian Journal of Remote Sensing, 40(3), 192-212.

Wulder, M.A., Masek, J.G., Cohen, W.B., Loveland, T.R., & Woodcock, C.E. (2012). Opening the archive: How free data has enabled the science and monitoring promise of Landsat. Remote Sensing of Environment, 122(0), 2-10.

Vågen, T.-G., Winowiecki, L.A., Tamene, D.L., & Tondoh, J.E. (2015). The Land Degradation Surveillance Framework (LDSF). In F.G. v4.1. (Ed.) (p. 14). World Agroforestry Centre, Nairobi, Kenya,

Zhang, X., Liao, C., Li, J., & Sun, Q. (2013). Fractional vegetation cover estimation in arid and semi-arid environments using HJ-1 satellite hyperspectral data. International Journal of Applied Earth Observation and Geoinformation, 21(0), 506-512.

Zhu, X., & Liu, D. (2014). Improving forest aboveground biomass estimation using seasonal Landsat NDVI time-series. ISPRS Journal of Photogrammetry and Remote Sensing(0)

Zhu, Z., Wang, S., & Woodcock, C.E. (2015). Improvement and expansion of the Fmask algorithm: cloud, cloud shadow, and snow detection for Landsats 4–7, 8, and Sentinel 2 images. Remote Sensing of Environment, 159, 269-277.

Zhu, Z., & Woodcock, C.E. (2014). Continuous change detection and classification of land cover using all available Landsat data. Remote Sensing of Environment, 144(0), 152-171.

Zhu, Z., Wulder, M.A., Roy, D.P., Woodcock, C.E., Hansen, M.C., Radeloff, V.C., Healey, S.P., Schaaf, C., Hostert, P., Strobl, P., Pekel, J.-F., Lymburner, L., Pahlevan, N., & Scambos, T.A. (2019). Benefits of the free and open Landsat data policy. Remote Sensing of Environment, 224, 382-385.

Zomer, R.J., Neufeldt, H., Xu, J., Ahrends, A., Bossio, D., Trabucco, A., van Noordwijk, M., & Wang, M. (2016). Global Tree Cover and Biomass Carbon on Agricultural Land: The contribution of agroforestry to global and national carbon budgets. Sci Rep, 6, 29987.